January 2012

Coordination Of 2,6-Bis(8′-Quinolinyl)pyridine On Rhenium(i) And Photochemistry Of Cyclopentadienyl Tricarbonyl Molybdenum Dimer With Arene Disulfides

Clayton Bosworth

COORDINATION OF 2,6-BIS(8′-QUINOLINYL)PYRIDINE ON RHENIUM(I) AND PHOTOCHEMISTRY OF CYCLOPENTADIENYL TRICARBONYL MOLYBDENUM DIMER WITH ARENE DISULFIDES

by

Clayton J. Bosworth

Bachelor of Science, University of North Dakota, 2008

A Thesis

Submitted to the Graduate Faculty

of the

University of North Dakota

In partial fulfillment of the requirements

for the degree of Master of Science

Grand Forks, North Dakota

May

2012

This thesis submitted by Clayton J. Bosworth in partial fulfillment of the requirements for the Degree of Master of Science from the University of North Dakota, has been read by the Faculty Advisory Committee under whom the work has been done and is hereby approved.

(Chairperson) Sean E. Hightower

Harmon B. Abrahamson

Lothar Stahl

This thesis meets the standards for appearance, conforms to the style and format requirements of the Graduate School of the University of North Dakota, and is hereby approved.

Wayne Swisher Dean of the Graduate School

April 18, 2012

Date

PERMISSION

Title: Coordination of 2,6-bis(8′-quinolinyl)pyridine on Rhenium(I) and Photochemistry of Cyclopentadienyl Tricarbonyl Molybdenum Dimer with Arene Disulfides

Department: Chemistry

Degree: Master of Science

In presenting this thesis in partial fulfillment of the requirements for a graduate degree from the University of North Dakota, I agree that the library of this University shall make it freely available for inspection. I further agree that permission for extensive copying for scholarly purposes may be granted by the professor who supervised my thesis work or, in his absence, by the Chairperson of the department or the Dean of the Graduate School. It is understood that any copying or publication or other use of this thesis or part thereof for financial gain shall not be allowed without my written permission. It is also understood that due recognition shall be given to me and to the University of North Dakota in any scholarly use which may be made of any material in my thesis.

Signature Clayton J. Bosowrth

Date April 18, 2012

TABLE OF CONTENTS

LIST OF FIGURES

LIST OF SCHEMES

LIST OF TABLES

ACKNOWLEDGEMENTS

I would like to thank my committee members for guidance and patience over the years. Their assistance and wisdom was greatly appreciated in facing the many challenges along the way.

I am indebted to my advisors for all the skills I have learned with the advanced tools they provided. Besides operating equipment, they paved the way for interpreting the data and the challenge to present it in a clear fashion.

The support of my family and friends cannot go unmentioned. They provided the understanding of long hours away, unwavering support, and a warm environment for regrouping all in stride.

I would also like to thank the Chemistry Department and staff for their assistance and opportunities to spread the wonders of chemistry.

ABSTRACT

An ideal photosensitizer should have an excited state with high energy and sufficiently long lifetime to promote electron and/or energy transfer processes. Many *facial*-tricarbonyl Re(I)-diimine complexes have demonstrated sufficiently long lifetimes to photosensitize many reactions. However, these complexes only utilize small portions of the visible spectrum, thereby diminishing their overall effectiveness. Recent work has resulted in opening a synthetic route to the meridionally tris-chelated *mer,cis*-Re(tpy-κ^3N)$(CO)_2Cl$ (tpy = 2,2′:6,2-terpyridine) complex which absorbs light throughout the entire visible spectrum. However, as with many other metal-terpyridine complexes, the *mer,cis*-[Re(tpy-κ^3N)$(CO)_2L]^{n+}$ (L = $NCCH_3$, PPh_3, NC_5H_5, PEt_3, and Cl; n = 0 or 1) failed to produce emission at room temperature.

The 2,6-bis(8′-quinolinyl)pyridine (bqp) ligand has been shown to form meridionally tris-chelated complexes with Ru(II) with observed room temperature emissions on the order of 3 μs. Results from our laboratory suggest that the *mer,cis*-Re(bqp-κ^3N)$(CO)_2Cl$ complex is expected to absorb light throughout the entire visible spectrum at molar absorptivities greater than the

mer,cis-Re(tpy-κ^3*N*)$(CO)_2Cl$. This study details initial coordination studies of the 2,6-bis(8′-quinolinyl)pyridine to Re(I).

The photochemistry of the molybdenum dimer $[CpMo(CO)_3]_2$ with organic disulfides were investigated. Broad-band light sources were used for synthesis of the Mo-S containing products. Products were characterized by infrared and ^{1}H–NMR techniques. Isolation of pure product allowed determination of UV-visible absorption parameters. These parameters were used to determine quantum yields under monochromatic irradiation.

CHAPTER 1.

INTRODUCTION

1.1 General Photochemistry

Photochemical processes have been of great interest to scientists since the discovery of photosynthesis. This interest has been around as an organized subfield of chemistry for more than a century. The main concern in photochemistry is the study of electronically excited states of molecules, which provide many unique reactions. These excited states are reached by the energy provided from a photon or quantum of light. The processes induced by the excited states fall into two classes of reactions based on its course along the potential energy surface, adiabatic or diabatic.[1] For an adiabatic reaction, the chemical change occurs on the same continuous potential energy surface, whereas crossing potential surfaces is classified as a diabatic reaction, Figure 1. The photodissociation of small molecules in the vapor state, $I_2 + h\nu \rightarrow I^* + I$, and proton transfer in the excited state are two examples of adiabatic processes. For this to happen, the reactants and products need to correlate with one another and the transition state. This means the product will be in an electronic excited state

and detectable by luminescence and/or photochemical properties. However, an intermediate can interfere with the formation of the product. While this form of activation provides different states than thermal activation, the states are not without limitations.[1]

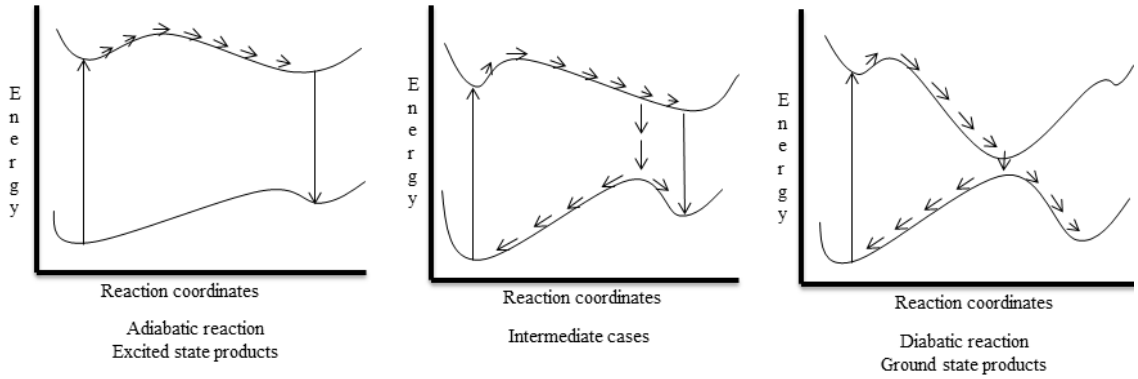

Figure 1. Classification of photochemical processes based on potential energy surfaces (ref. 1).

The first law of photochemistry states that only the light absorbed by a molecule can be effective in producing photochemical change in a molecule. This law is based on the works of Grotthuss (1817) and Draper (1843).[1b]

The quantum yield is determined from the yield of photochemical product. For the general equation; A + $h\nu \rightarrow$ B, the quantum yield is defined by

$$\Phi_B = \frac{\text{Molecules of B formed}}{\text{Quanta of light absorbed by A}}$$

The numerator is found by conventional chemical analysis. The denominator is calculated from the measured total energy of the absorbed light of wavelength λ and assuming that each quantum has energy equal to $h\nu$.[1,2]

The second law of photochemistry deduced by Stark (1908-1912) and Einstein (1912-13) states the absorption of light by a molecule is a one-quantum process, so the sum of the primary process quantum yields Φ must be unity; that is $\Sigma\Phi_i = 1.00$, where Φ_i is the quantum yield of the *i*th primary process. These primary processes may include dissociation, phosphorescence, fluorescence, radiationless transitions, isomerization, and all other reaction paths which lead to the destruction or deactivation of the excited molecule.[1b]

1.2 Photochemistry of Metal Coordination Compounds

The use of transition metal complexes in photochemistry has been studied for many years.[3,4] Most transition metal excited states can be easily categorized as two types:[5] ligand field or charge transfer. The difference in the electronic states comes from the composition of the orbitals involved in the transition. For ligand field excited states, both the starting and ending orbitals are predominately metal d-orbital in character. On the other hand, a charge transfer excited state has significant amount ligand contribution to one or the other of the orbitals. The processes generated by these states are as follows:[5]

(1) Substitutional (S = solvent species, L = Ligand)

$$*ML_6 + S \rightarrow ML_5S + L$$

(2) Isomerization (AA = bidentate of two monodentate ligands)

$$*(cis \text{ or } trans;\ \Delta \text{ or } \Lambda);\ M(AA)_2XY \rightarrow (trans \text{ or } cis;\ \Lambda \text{ or } \Delta)\ M(AA)_2XY$$

(3) Deactivation

$$*ML_6 \rightarrow ML_6 + \text{heat}$$

(4) Radiative

$$*ML_6 \rightarrow ML_6 + h\nu$$

(5) Oxidation-reduction (·L = free radical)

$$*M(III)L_6 + S \rightarrow M(II)L_5S + \cdot L$$

The ligand field states can initiate processes 1–4. A charge transfer excited state can initiate any of the processes.

The main process that will be of interest for the systems in Chapter 2 is oxidation-reduction resulting from a charge-transfer excited state. The light energy absorbed by the compound excites electrons to higher energy states that enable the reduction of molecules like carbon dioxide or water; in the process the metal center is oxidized. The system in Chapter 3 uses a special ligand-field excitation process that relies on two metals.

CHAPTER 2.

COORDINATION OF 2,6-BIS(8′-QUINOLINYL)PYRIDINE ON RHENIUM(I)

2.1 Introduction

Some transition metal diimine complexes have shown to be beneficial in electron or energy transfer processes required for photosensitizers.[6-9] An ideal photosensitizer should have an excited state with high energy and sufficiently long lifetime to promote these processes. There has been a lot of focus towards Ru(II) and Os(II)-diimine complexes for these desired processes.[10] The use of *fac*-tricarbonyl Re(I)-diimine complexes have also shown similar results that are desirable for photosensitizing reactions.[10-12] The drawback of these Re(I)-complexes is the limited absorption of the visible spectrum of light, which reduces their overall effectiveness. One way to improve visible absorption has led to the chelation of tridentate amine ligands.[6,10]

A compound that has proven capable of this is *mer,cis*-Re(tpy-κ^3N)$(CO)_2Cl$ (tpy = 2,2′:6,2-terpyridine).[10] However, as with many other metal-terpyridine complexes, the *mer,cis*-$[Re(tpy\text{-}\kappa^3N)(CO)_2L]^{n+}$ (L = PPh_3, NC_5H_5, PEt_3, and Cl; n = 0 or 1) failed to produce emission at room temperature.[13,14] The decay at room-

temperature can be related to the energy gap law.[15] Some strategies used to remedy the failed emission in similar trisdentate ruthenium(II) complexes include (a) electron accepting and/or donating substituents,[16-18] (b) ligands with extended π-systems,[18-21] (c) cyclometalating or other strong σ-donor ligands,[18,22-24] and (d) bichromophoric systems[18,25], Figure 2.

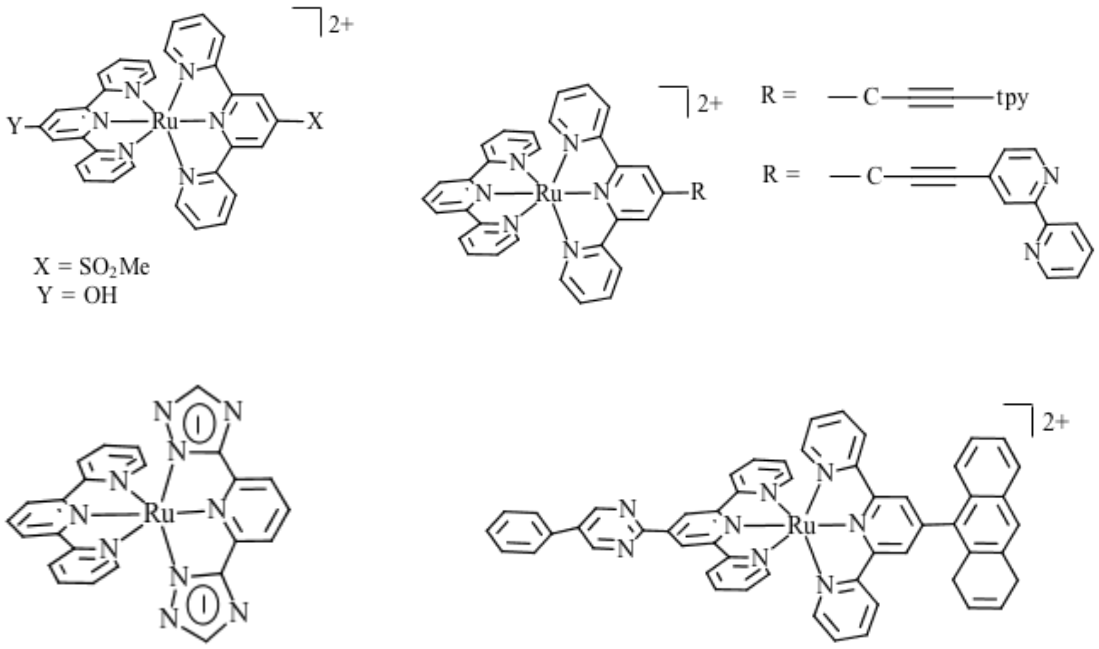

Figure 2. Structures of (a) top left,[26] (b) top right,[28] (c) bottom left,[34] and (d) bottom right.[18]

The 2,6-bis(8′-quinolinyl)pyridine (bqp) ligand has been shown to form meridionally (*mer*) tris-chelated complexes with Ru(II), with observed room temperature emissions on the order of 3 μs.[6] Abrahamsson *et al*. suggested the longer lifetimes were observed due to a greater difference of energy between a

triplet metal-to-ligand charge transfer (^{3}MLCT) and triplet metal-centered states (^{3}MC), Figure 3. The ^{3}MLCT state is the desired excited state, since it generates the energy or electron transfer and the ^{3}MC state allows the deactivation of the excited state through nonradiative means or ligand substitution.

To the best knowledge of the writer, there has been no reported attempt to coordinate the relatively new ligand, 2,6-bis(8′-quinolinyl)pyridine, onto rhenium(I). This work investigates methods for coordinating bqp ligand, in addition to accessing the reactivity of *fac*-[Re(bqp-κ^2*N*)(CO)$_3$L]$^{n+}$ (L = $NCCH_3$, PPh_3, NC_5H_5, PEt_3, and Cl; n = 0 or 1) complexes.

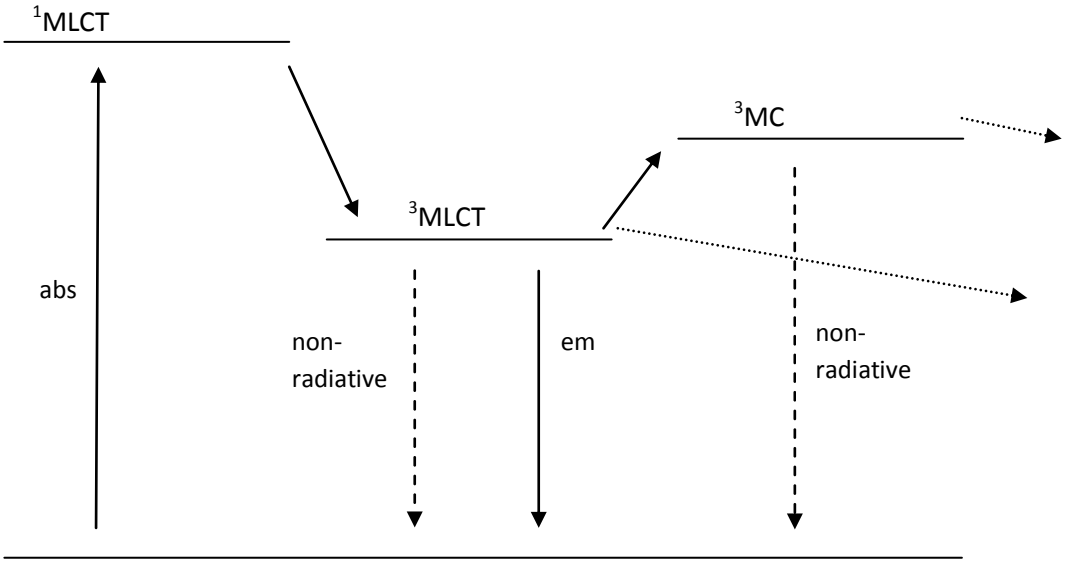

Figure 3. Excited state diagram for typical Ru(II) polypyridine complexes. Dotted lines denote photochemical reactions (refs. 7, 26).

2.2 Results

2.2.1 Preparation of Compounds

The synthesis of the 2,6-bis(8′-quinolinyl)pyridine (bqp) ligand followed the method reported in the literature (Scheme 1).[6,7] The only change made was a recrystallization of the off-white product from CH_2Cl_2 with diethyl ether instead of purification by column chromatography. This gave comparable yields and reduced preparation time for the ligand. An outline of the rhenium tricarbonyl synthesis is given in Scheme 2. The approach was to coordinate bqp on $Re(CO)_5Cl$ by replacing CO as reported previously.[10,11] The removal of chloride from *fac*-Re(bqp-κ^2*N*)$(CO)_3Cl$ (Figure 4) was effected by use of silver triflate, $Ag(CF_3SO_3)$, in acetonitrile, yielding *fac*-[Re(bqp-κ^2*N*)$(CO)_3(NCCH_3)$][CF_3SO_3] (Figure 4).[11] The silver chloride was easily removed from by filtration.

Scheme 1 Synthesis of the 2,6-bis(quinolinyl)pyridine (bqp) ligand

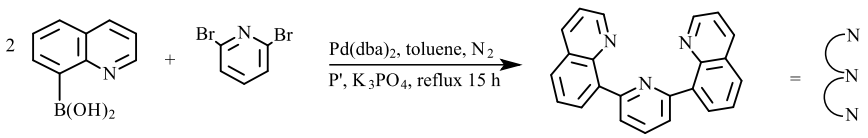

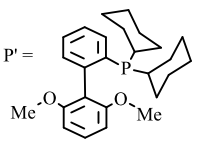

Scheme 2 Coordination of bqp on Re and reactivity of Re tricarbonyls

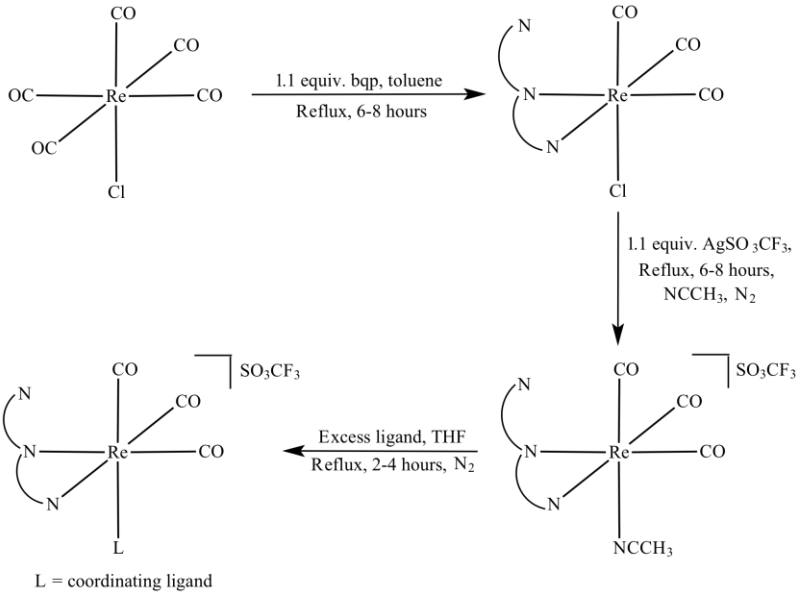

L is NC_5H_5 or PPh_3

fac-[Re(bqp-κ²*N*)(CO)₃(NCCH₃)][CF₃SO₃] was stable and was isolated and used in subsequent reactions with coordinating ligands. The approach was to remove acetonitrile from *fac*-[Re(bqp-κ²*N*)(CO)₃(NCCH₃)][CF₃SO₃] and replace it with pyridine or triphenylphosphine as previously reported (Figure 5).[10,11,13]

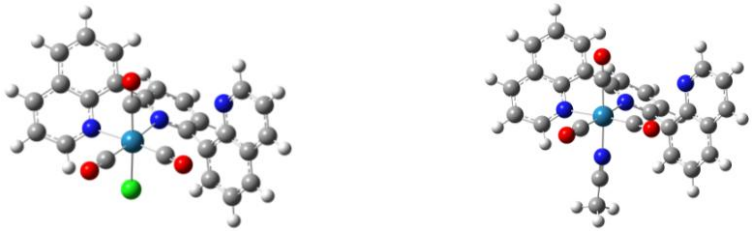

Figure 4. Ball and Stick Diagram of *fac*-Re(bqp-κ²*N*)(CO)₃Cl (**1**) [left] and *fac*-[Re(bqp-κ²*N*)(CO)₃(NCCH₃)]⁺ (**2**) [right].

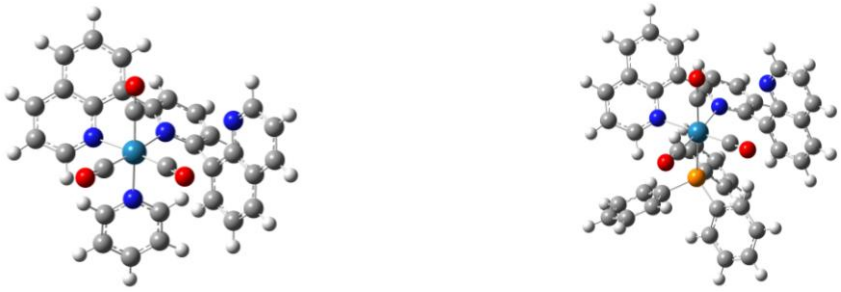

Figure 5. Ball and Stick Diagram of Target Products *fac*-[Re(bqp-κ^2*N*)(CO)$_3$(NC$_5$H$_5$)]$^+$ (**3**) [left] and *fac*-[Re(bqp-κ^2*N*)(CO)$_3$(PPh$_3$)]$^+$ (**4**) [right].

2.2.2 Absorption and Emission Studies

Absorption spectra were examined in acetonitrile and are listed in Table 2. Electron transitions are illustrated in Figure 6. The broad, low-energy peak, with extinction coefficients on the order of 10^2–10^4, was assigned as d$\pi \rightarrow \pi^*$.[27] The sharp peak at higher energy was assigned as $\pi \rightarrow \pi^*$, with extinction coefficients on the order of 10^5–10^7. Extinction coefficients observed for the complexes range from 9691 to 18800 M^{-1} cm^{-1} for the d$\pi \rightarrow \pi^*$ transition. The $\pi \rightarrow \pi^*$ transition gave extinction coefficients of 12439 to 23310 M^{-1} cm^{-1}. Complexes **1** and **2** have a Gaussian shape for the d$\pi \rightarrow \pi^*$ transitions due to the average absorption transitions. Whereas, complexes **3** and **4** have a shoulder growing in at lower energy on the d$\pi \rightarrow \pi^*$ peak and are identical to one another.

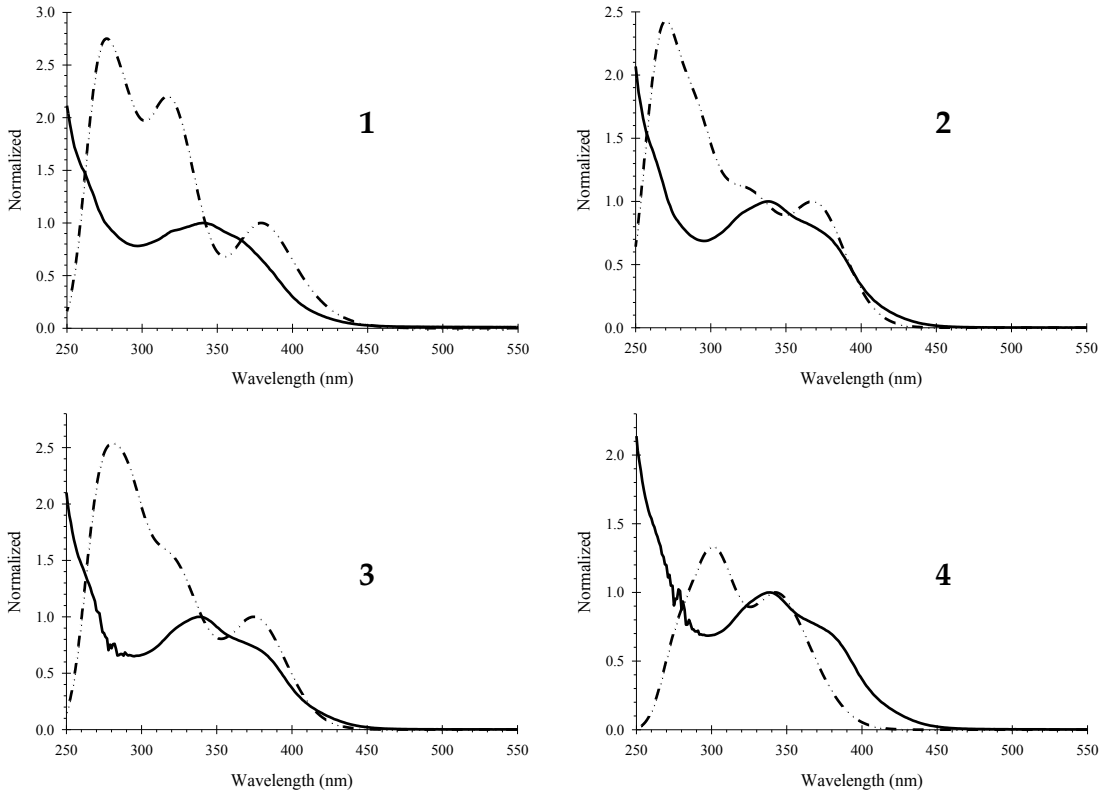

Figure 6. Experimental (—) and calculated spectra (– · · –) in acetonitrile.

Table 1. Absorption Energies (nm), Coefficients (M^{-1} cm^{-1}), Emissions (nm), and Intensities (a. u.) for Re Complexes

Compound	λ	ε	λ_{ex}	λ_{em}	I
1	267	17369			
	320	12439			
	338	13746			
	375	9691	370	593.97	39.733
2	267	18631			
	320	14048	315	597.94	27.01
	342	15608			
	375	11612	380	597.94	30.778
"3"	267	17978	290	303.07	13.759
	320	12872		598.97	22.43
	338	14029	338	593.97	52.099
	375	10845	375	597.05	54.112
"4"	267	23310	300	597.94	36.666
	320	16297			
	338	18800	338	597.94	35.225
	375	13676	375	597.94	41.333

The emission spectra were obtained at room temperature in acetonitrile. The emission maxima are presented in Table 1. All complexes showed nonstructured emissions as seen in Figure 7. The room-temperature emission spectra were initially weak in intensity; this was suspected to be due to O_2-quenching of the excited state energy. Argon was bubbled through the solutions to remove oxygen and intensities were improved. Nonstructured emission was previously observed for rhenium tricarbonyl complexes and was assigned to ^{3}MLCT-based emission.[38]

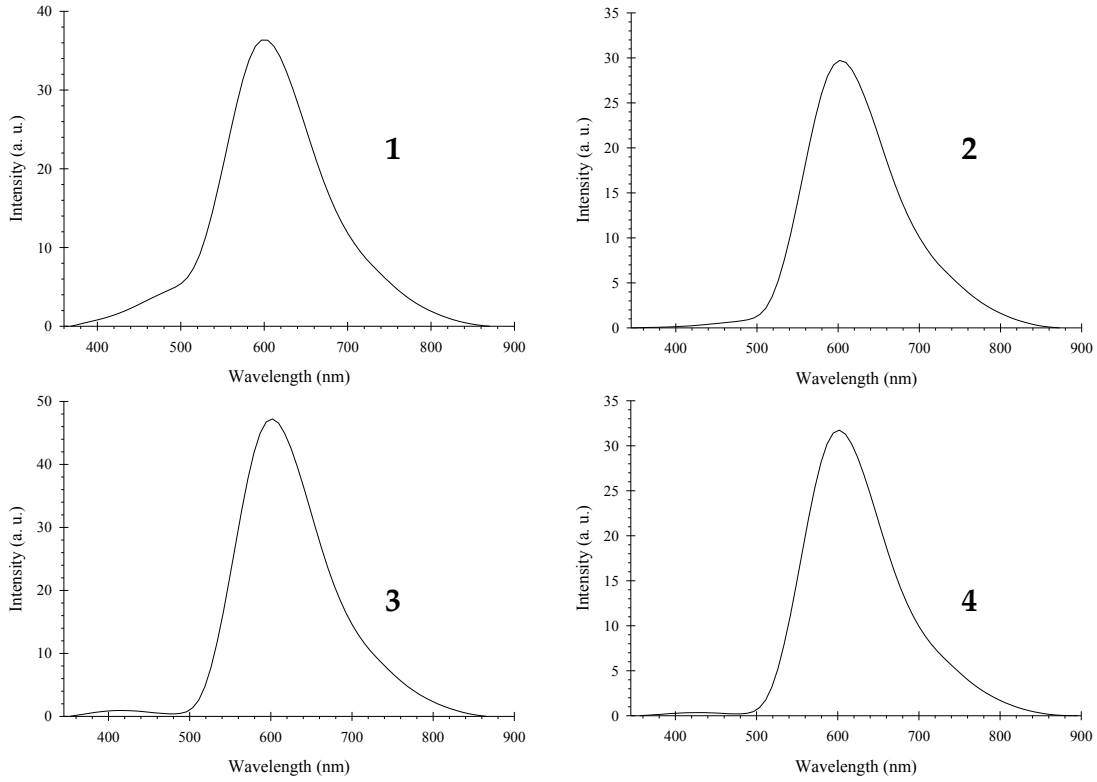

Figure 7. Room-temperature emission of (**1**) 8.237 x 10^{-5} M, (**2**) 1.129 x 10^{-4} M, (**3**) 6.901 x 10^{-5} M, and (**4**) 5.025 x 10^{-5} M in acetonitrile.

2.2.3 Nuclear Magnetic Resonance Studies

NMR data was collected in CD_2Cl_2 and presented in Table 3. The spectra are shown in Appendix A. The proton resonances of the pyridine ligand (protons 3, 4, and 5) were found in between those of the quinoline ring (2′, 2″, 3′, 3″, 4′, 4″, 5′, 5″, 6′, 6″, 7′, and 7″). The resonance for all protons are shifted downfield for *fac*-Re(bqp-κ^2*N*)$(CO)_3Cl$ compared with the protons from the free bqp ligand. Replacement of Cl^- by $NCCH_3$ causes a further downfield shift of protons 2′ and 2″ and protons 3′, 3″, 4′, 4″, 7′, 7″ are shifted slightly upfield. The remaining aromatic proton resonances are not affected. The proton resonance of acetonitrile is shifted downfield when coordinated on rhenium. Attempted replacement of $NCCH_3$ with NC_5H_5 or PPh_3 did not causes any change in proton resonance of the bqp ligand and no proton resonance of NC_5H_5 or PPh_3 was present.

Table 2. NMR Data with Assignment of Protons

Complex	2′, 2″	4′, 4″, 7′, 7″	3, 5	4, 5′, 5″	6′, 6″	3′, 3″	ligand	
bqp	8.97, dd,	8.26, m	8.12, d,	7.92, m	7.68, dd,	7.48, dd,		
	(*J* = 4.1, 1.9 Hz)		(*J* = 7.8 Hz)		(*J* = 8.2, 7.2 Hz)	(*J* = 8.3, 4.1 Hz)		
1	9.68, dd,	8.69, dd,	8.55, dd,	8.25, m	7.98, dd,	7.90, m		
	(*J* = 5.0, 1.6 Hz)	(*J* = 8.2, 1.5 Hz)	(*J* = 7.2, 1.4 Hz)		(*J* = 8.1, 7.4 Hz)			
2	9.87, dd,	8.65, dd,	8.54, dd,	8.23, m	7.97, m	7.87, d,	2.54, d,	2.43, m
	(*J* = 5.2, 1.6 Hz)	(*J* = 8.2, 1.6 Hz)	(*J* = 7.3, 1.4 Hz)			(*J* = 8.1 Hz)	(*J* = 11.3 Hz)	
"3"	9.87, dd,	8.65, dd,	8.54, dd,	8.23, m	7.97, m	7.87, d,		
	(*J* = 5.0, 1.6 Hz)	(*J* = 8.3, 1.5 Hz)	(*J* = 7.3, 1.4 Hz)			(*J* = 8.1 Hz)		
"4"	9.87, dd,	8.65, dd,	8.54, dd,	8.23, m	7.97, m	7.87, d,		
	(*J* = 5.0, 1.6 Hz)	(*J* = 8.3, 1.5 Hz)	(*J* = 7.4, 1.4 Hz)			(*J* = 8.1 Hz)		

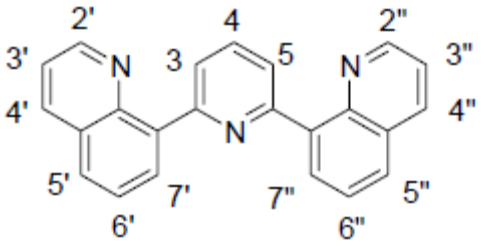

2.2.4 Infrared Studies

The energy of the carbonyl stretches for the complexes are shown in Table 4 and the spectra examined in acetonitrile are shown in Figure 8. The symmetry of the carbonyls around the Re(I) center leads to distinct bands in the carbonyl region (ν(CO), 2200-1800 cm^{-1}). The *fac*-$[Re^{I}(L\text{-}\kappa^{2}N)(CO)_3L']^{n+}$ (where L = 2,2′:6,2-terpyridine, 2,2′-bipyrazine (bpz), or bipyridine (bpy), L′ = $NCCH_3$, NC_5H_5, Cl, or PPh_3, and n = 0 or 1) complexes typically exhibit three peaks in the carbonyl region.[11,12,27] There were only two carbonyl peaks for all complexes examined here. This was attributed as the two asymmetric IR bands having energies too close together for separation creating a broad Gaussian-shaped peak. The bands for complex **2** shift to higher energy compared to complex **1**, while vibrational peaks for complexes **3** and **4** did not change significantly from complex **2**.

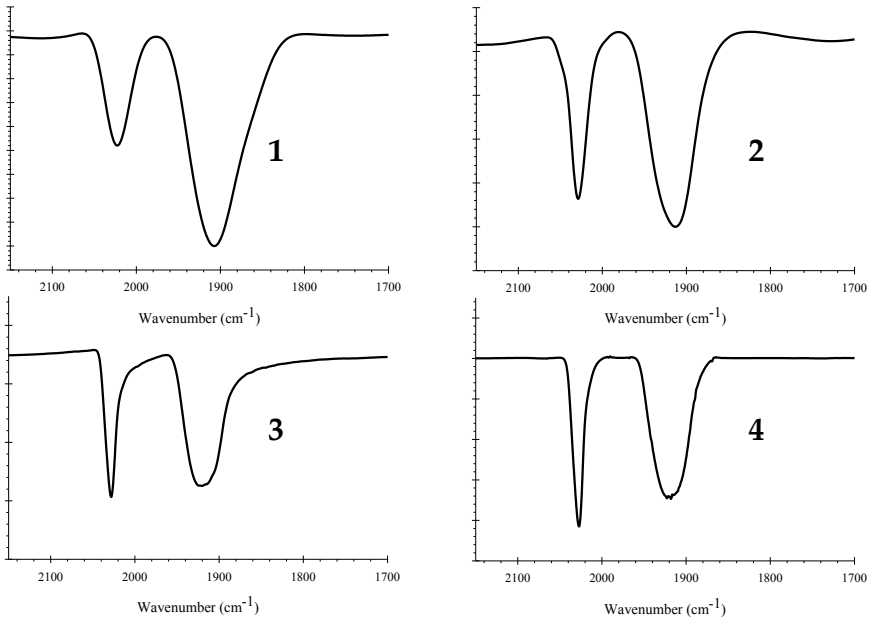

Figure 8. IR spectra of the carbonyl stretch region.

Table 3. Experimental and Calculated Carbonyl Stretch Frequencies (cm^{-1})

	expt'l	calc'd	tpy[21]	bpz[22]	bpy[36]		expt'l	calc'd[a]	bpy[29b]
1	2020	2087.25	2024	2049	2022	**3**	2028	2097.53	2040
	–	1976.39	1920	1939	sh		1919	1988.42	1950
	1902	1960.43	1898	1915.8	1890		–	1984.21	–
2	2028	2103.33	2040		2026	**4**	2028	2097.99	
	1918	2000	1941		sh		1923	1999.17	
	–	1994.76	1930		1906		1918	1979.4	

[a]Calculations performed on target compounds

2.2.5 Mass Spectrometric Studies

The parent peaks are presented in Table 4. The samples were run as 1 ppm solution in 50% methanol/H_2O with 10 mM acetic acid as ionization agent and a 250 V fragmentor voltage. The calculated parent peaks were generated via the ChemDoodle computer program.[29]

Table 4. Mass Spectrometric Data

	calc'd	expt'l
1	639.0330	604.0646
2	645.0906	604.0645
3	683.1062	604.0648
4	866.1552	604.0645

2.2.6 Crystal Structures

Crystals for complex **2** were grown by slow diffusion of benzene in acetonitrile. The crystals of *fac*-[Re(bqp-κ^3N)$(CO)_3]^+$ were grown by slow diffusion of benzene or diethyl ether in acetonitrile and slow evaporation of CH_2Cl_2/CD_2Cl_2 mixtures.

2.2.7 Computational Studies

The singlet ground state geometries of the complexes **1** through **5** were optimized in acetonitrile (CH_3CN) using Conductor-like Polarizable Continuum Model (CPCM) — Self-Consistent Reaction Field (SCRF)[30] using the B3LPY[31] functional as implemented in the GAUSSIAN 09 program package.[32] The LANL2DZ ECP[33-36] was used for the Re effective core potential (ECP). This ECP effectively puts the all electron 6-311G* basis set on the valance shell of Re.[37] Mixed basis set calculations using 3-21G* for H atoms and 6-311G* for all other atoms were used in order to provide molecular structure and energies of the complexes at a reduced computational cost (Appendix D). All stationary points were characterized by frequency calculations (*i.e.*, the absence of negative frequencies) performed at the same level.

Molecular orbital (MO) compositions and the overlap populations were calculated using the AOMix program[38,39] and the Mullikan scheme.[40-43] Atomic charges were calculated using the Mullikan and natural population analyses[44] (MPA and NPA, respectively) as implemented in GAUSSIAN 09. The analysis of the MO compositions in terms of occupied and unoccupied fragment molecular orbitals (OFOs and UFOs, respectively), construction of orbital interaction diagrams, the charge decomposition analysis (CDA), and the extended charge decomposition analysis (ECDA) were performed using AOMix-CDA.[39,45]

Non-equilibrium TDDFT[46]/CPCM-SCRF calculations were employed to produce a number of singlet excited-states for complexes **1** through **4** and the product *fac*-[Re(bqp-κ^3*N*)(CO)$_3$]$^+$ in CH_3CN based on the singlet ground-state geometry (Appendix B). The output contained information for the excited state energies and oscillator strengths (*f*) and a list of the excitations that give rise to each excited-state, the orbitals involved, as well as the wave function coefficients of the excitations.

A number of triplet excited states for complexes **1** through **4** and *fac*-[Re(bqp-κ^3*N*)(CO)$_3$]$^+$ were calculated based on the triplet ground-state geometry using non-equilibrium TDDFT[46]/CPCM-SCRF calculations (in CH_3CN).

2.3 Discussion

2.3.1 Absorption and Emission Studies

As noted in the Results section, complexes **1**–**4** showed an intense absorption in the UV, ~230 nm, and a broad, less intense band, 390–420 nm. Complex **2** started to extend further into the visible region, 400–800 nm. The spectra of complexes **3** and **4** were identical. The MLCT absorptions are similar to previously reported bis–chelated diimine Re(I) complexes.[8,23,24] However, the extinction coefficients observed for all Re(bqp-κ^2*N*) complexes here are larger in magnitude than before.[11,12,27,28]

Emission spectra were taken at room-temperature and all complexes showed nonstructured emission with similar energy. These nonstructured emission manifolds were assigned as ^{3}MLCT emitters.[28b] With all complexes having similar energies of emission, the coordinated ligand shows little effect on the Re^I(bqp-κ^2*N*) centers.

2.3.2 Nuclear Magnetic Resonance Studies

The coordination of the bqp ligand on Re(I) was successful, as a downfield shift is seen in the aromatic region of the NMR spectrum. For complex **1**, the electron density present on the bqp ring in the HOMO primarily resides on the 2, 3, and 4 positions on the quinoline rings. Consequently, the influence of acetonitrile coordinated on the metal causes the electron density to shift onto all positions of the quinoline rings. When comparing complex **1** with **2**, it was observed that a small upfield shift in the aromatic region and the downfield shift of coordinated acetonitrile. However, complexes **3** and **4** showed small shifts of aromatic protons when compared to complex **2** and no ligand proton peaks of pyridine, triphenylphosphine, or acetonitrile. Since the hydrogens in the in the aromatic region are assigned to the bqp ring and acetonitrile is not coordinated anymore, the reactions to coordinate pyridine or triphenylphosphine did not proceed as expected.

2.3.3 Infrared Studies

The carbonyl region, 2200–1800 cm^{-1}, was the focus of IR studies for monitoring the progress of reactions, since the only vibrations present are from carbonyls, and characterizing structures. Rhenium(I) tricarbonyl complexes have exhibited three peaks in this region.[47,48] Group theory analysis assigned these to the $2A_1 + B_2$ modes.[49-52] The calculations for all complexes show the symmetric and one asymmetric peak involve all three carbonyl groups and the second asymmetric peak involves only the two equatorial carbonyls. The lowest energy vibration is an asymmetric stretch involving all three carbonyl groups. The second lowest vibration involves two carbonyl groups and the highest vibration is the symmetric stretch involving all three carbonyl groups.

The complexes **1**–**4** showed only two peaks, one sharp and one broad. The broad peak was reasoned to be the result of the close proximity of the two asymmetric bands causing a broad, Gaussian-shaped peak. As seen in Table 3, complex **1** showed maxima at 2020 and 1902 cm^{-1}, while complex **2** shifted to higher energy at 2028 and 1918 cm^{-1}. However, complexes **3** and **4** did not change from the starting material, *fac*-[Re(bqp-κ^2*N*)$(CO)_3(NCCH_3)]^+$, and were within experimental error. Also shown in Table 3, the carbonyl stretches of similar bis–chelated diimine Re(I) tricarbonyl complexes are presented for

comparison.[10,11,26] A similar shift in vibration energy with ligand replacement of chloride with acetonitrile is seen toward higher energy. This phenomenon is attributed to weakening of the metal backbonding to the carbonyls, when the electron density is increased at the metal center.

2.3.4 Mass Spectrometric Studies

All complexes showed parent peaks at 604 a.u. experimentally. From UV-Vis., IR, and NMR data, complexes **1** and **2** were synthesized successfully. Upon ionization in the MS, the complexes fragment and recombine in varying combinations. For complex **1**, the *fac*-[Re(bqp-κ^3*N*)$(CO)_3]^+$ fragment is produced from loss of Cl^- accounts for a m/z 604 peak. Complex **2** is a charged complex; however, acetonitrile is a very labile ligand quickly giving rise to the fragment with m/z 604. Complexes **3** and **4** are charged also, but their results are inconsistent with the expected m/z for coordination of pyridine (m/z 683) and triphenylphosphine (m/z 866) on Re(I) (Scheme 3). The mass shown for the complexes **3** and **4** is presumed to be *fac*-[Re(bqp-κ^3*N*)$(CO)_3]^+$.

Scheme 3 Attempted formation of substituted [Re(bqp-κ²*N*)(CO)₃L] complexes

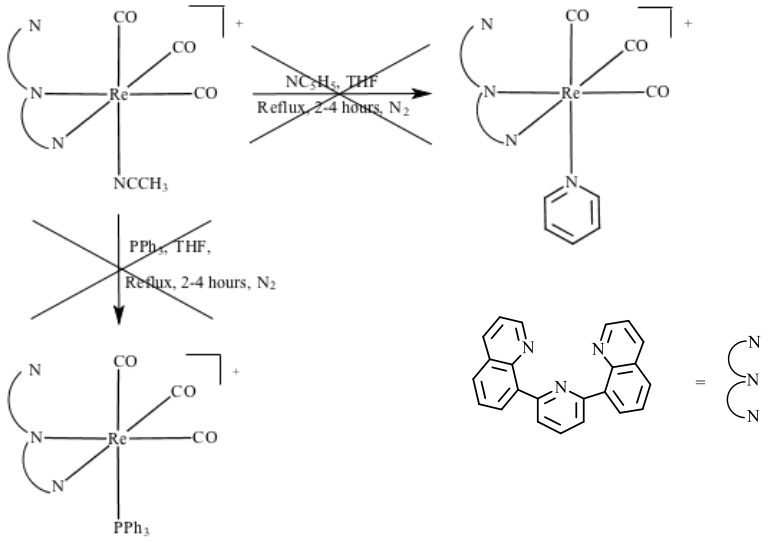

2.3.5 Crystal Structures

Recently, we were able to grow x-ray quality crystals for the product of the pyridine coordination reaction. Figure 9 shows a trischelated *fac*-[Re(bqp-κ³*N*)(CO)₃]⁺ complex that may be best described as having trigonal antiprismatic (distorted octahedral) geometry.

Figure 9. Crystal Structure of *fac*-[Re(bqp-κ³*N*)(CO)₃]⁺ (**5**).

2.3.6 Computational Studies

Geometry optimization and subsequent frequency calculations provide a convenient starting point in the elucidation of the experimental results. A number of singlet excited-states were computed based on the corresponding optimized singlet ground state geometries for complexes **1** through **5**. The four lowest lying excited-states are listed in Table 6 (while the remainder of the transitions are listed in Appendix B1). Mulliken populations were calculated for the singlet ground-state geometry for complexes **1** through **5** are shown in Table 7. The first four excited states were chosen based on the area of interest, which are the visible and the near-UV regions. Each of the corresponding complexes shows singlet excited-states that are essentially dominated by the frontier molecular orbital region. The HOMO, HOMO-1, and HOMO-2 for complexes **1** and **5** contained 40% or more Re_d character. For complexes **2** through **4**, the composition of these orbitals fluctuates between predominantly Re_d-based and bqp-based orbitals with notable CO-based contributions. The LUMOs for all complexes are dominated by bqp-based compositions (greater than 80% in all cases). The picture these data portrays is one that is consistent with excitations that are predominantly metal-to-ligand charge transfer (MLCT) or metal-ligand-to-ligand charge transfer (MLLCT). These results are similar to other Re(I) diimine complexes[23,37] and a Ru(II) triimine complex.[7]

Of particular interest is that complex **5** shows a sizable contribution of CO in the HOMO orbital which is the major contributor to the first excitation (Figure 10). This suggest that removal of electron density from the Re-CO bond could potentially be effected by excitation with light; thereby, labilizing CO to substitution.[53] This could potentially provide a pathway to the meridonally tris-chelated dicarbonyl complex *mer,cis*-Re(bqp-κ^3*N*)(CO)$_2$(NCCH$_3$)]$^+$ shown in Scheme 4. These studies are currently being conducted.

Table 5. Singlet Electronic Transitions for Re(I) complexes

#	λ, nm	f	Assignment MO#→MO#
			Complex 1
1	409.2	0.0110	124→125 (+96%)
2	393.5	0.0102	123→125 (+71%), 122→125 (28%)
3	377.6	0.0843	122→125 (+67%), 123→125 (+25%)
4	335.6	0.0410	121→125 (+94%)
			Complex 2
1	372.2	0.1140	126→127 (+94%)
2	356.9	0.0085	124→127 (+61%), 125→127 (36%)
3	344.5	0.0101	123→127 (+78%), 124→127 (13%), 125→127 (8%)
4	334.8	0.0792	125→127 (+53%), 124→127 (+23%), 123→127 (+19%)
			Complex 3
1	379.8	0.0870	136→137 (+83%), 135→137 (+12%)
2	369.3	0.0334	135→137 (+86%), 136→137 (11%)
3	349.5	0.0072	133→137 (+83%), 134→137 (+15%)
4	337.3	0.0620	134→137 (+79%), 133→137 (15%)
			Complex 4
1	363.9	0.0664	184→185 (+92%)
2	347.1	0.0033	182→185 (+78%), 181→185 (+11%)
3	343.1	0.1044	183→185 (+78%), 181→185 (+11%)
4	338.1	0.0484	181→185 (+46%), 180→185 (+21%), 182→185 (+17%), 183→185 (13%)
			Complex 5
1	395.1	0.1678	115→116 (+93%)
2	384.2	0.0206	115→117 (+84%), 113→116 (+11%)
3	375.9	0.0066	113→116 (+88%), 114→116 (10%)
4	360.4	0.0233	115→117 (+90%)

Table 6. Electron Distribution in % of Selected Orbitals of Re(I) Complexes

Orbital	Re_d	CO	bqp	L[a]
		Complex 1		
121	2	3	95	< 1
122	62	26	11	< 1
123	38	20	3	36
124	42	21	4	32
125	< 1	1	98	< 1
126	< 1	1	98	< 1
		Complex 2		
123	42	14	38	6
124	53	18	20	10
125	24	13	60	2
126	21	7	71	1
127	< 1	9	88	< 1
128	< 1	15	83	< 1
		Complex 3		
133	64	26	9	< 1
134	32	15	52	< 1
135	61	25	9	5
136	22	8	70	< 1
137	< 1	2	96	< 1
138	< 1	4	9	84
		Complex 4		
181	8	3	87	1
183	35	14	25	24
184	32	11	48	9
185	1	10	82	5
186	< 1	19	47	30
		Complex 5		
113	51	24	23	NA
114	34	13	53	NA
115	47	18	34	NA
116	< 1	2	96	NA
117	1	1	97	NA

[a]L = Cl^- (**1**), $NCCH_3$ (**2**), NC_5H_5 (**3**), and PPh_3 (**4**).

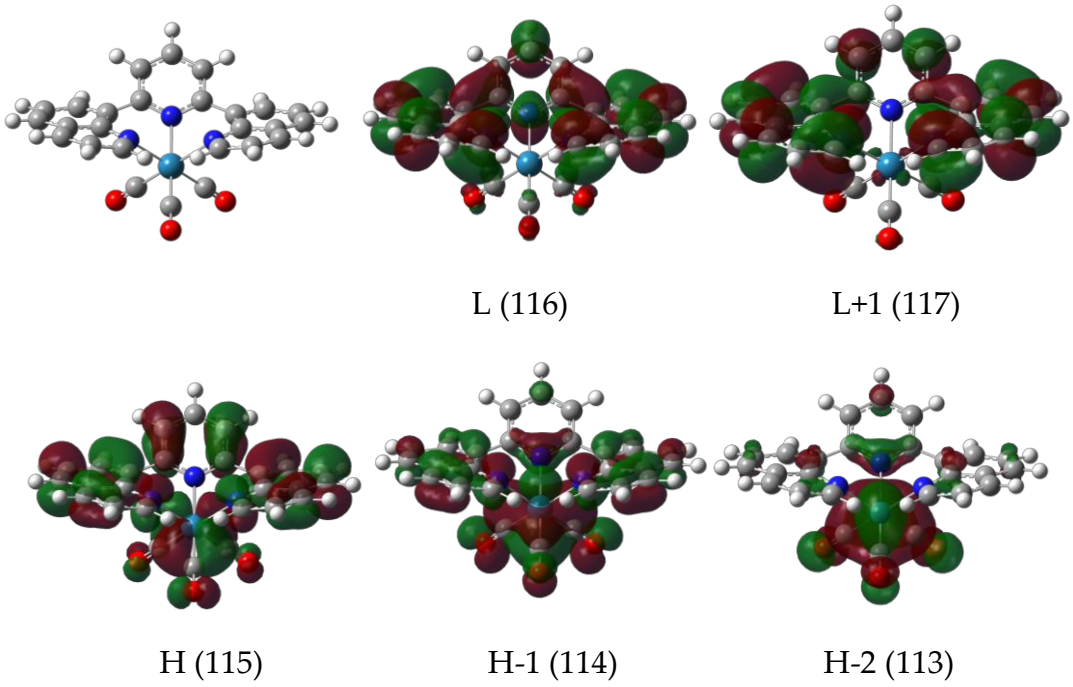

Figure 10. Schematic diagrams of frontier orbitals for *fac*-[Re(bqp-κ³*N*)(CO)₃]⁺ (**5**).

Scheme 4 Proposed pathway for photochemical reaction of complex **5**

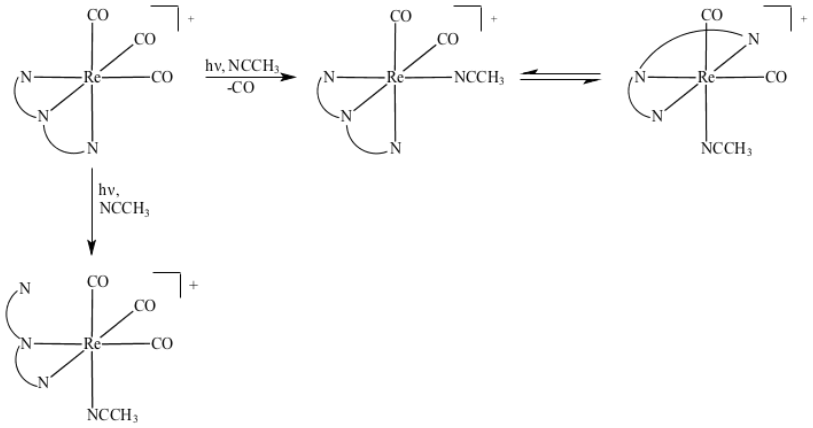

A number of triplet excited states were calculated for complexes **1–5** as well. The four low-lying triplet states are presented in Table 8 (while the remainder of the transitions are listed in Appendix B) since these transitions

occur in the visible region. According to this Kasha's rule, the emitting state will be the zero vibrational level of the lowest excited state.[1] The transitions generated by Gaussian 09 are singlet-triplet excitations. From the nonstructured emission in Figure 7, the relaxation is from a triplet state down to the ground state. Therefore, the emission is expected to exhibit bqp character.

The spatial distributions of the frontier orbitals for the *fac*-[Re(bqp-κ^3N)$(CO)_3]^+$ complex are shown in Figure 10. As can be seen from the figure, the HOMOs have major contributions from Re_d (30–50%) and bqp (20–50%). The LUMOs are dominated with bqp-based contribution (>95%).

Table 7. Calculated Triplet Excited States of Complexes **1–5** in Acetonitrile Based on Lowest Lying Triplet State Geometry

State	f	$\phi_o \rightarrow \phi_v$	type	E_{ver}
		Complex 1		
1	0.00	121 → 125, 122 → 125, 123 → 125, 124 → 125	Re_d, bqp, CO, Cl→bqp	497.14
2	0.00	121 → 127, 121 → 126	bqp →bqp	445.73
3	0.00	124 → 125	Re_d, CO, Cl → bqp	417.28
4	0.00	123 → 125	Re_d, Cl, CO → bqp	399.95
		Complex 2		
1	0.00	125 → 127, 126 → 127	bqp, Re_d →bqp, CO	496.03
2	0.00	126 → 128, 127 → 129	bqp →bqp	443.58
3	0.00	122 → 127, 124 → 127, 126 → 127	Re_d, bqp, CO → bqp	377.52
4	0.00	124 → 127, 123 → 127	Re_d, bqp, CO → bqp	363.89
		Complex 3		
1	0.00	134 → 137, 136 → 137	bqp, Re_d, CO → bqp	498.26
2	0.00	134 → 140, 136 → 138	bqp, Re_d, CO → bqp	443.83
3	0.00	135 → 137, 136 → 137, 132 → 137	Re_d, CO, bqp → bqp	388.54
4	0.00	132 → 137, 136 → 137	bqp, Re_d →bqp	369.25
		Complex 4		
1	0.00	183 → 185, 184 → 185	Re_d, bqp, PPh_3→bqp	486.73
2	0.00	184 → 186, 183 → 187	bqp, Re_d→bqp, CO, PPh_3	446.61
3	0.00	184 → 185, 182 → 185, 178 → 185	bqp, Re_d, PPh_3→bqp	375.72
4	0.00	182 → 185, 182 → 186, 183 → 185	bqp, Re_d →bqp, CO	364.21
		Complex 5		
1	0.00	115 → 116, 111 → 117, 114 → 117	Re_d, bqp, CO → bqp	514.60
2	0.00	115 →117, 111 → 116, 114 → 116	Re_d, bqp, CO → bqp	506.16
3	0.00	114 → 116, 113 → 116	Re_d, bqp, CO → bqp	396.25
4	0.00	113 → 116, 115 → 117	Re_d, bqp, CO → bqp	388.09

E_{ver} is the energy of the vertical transition in nm.

2.4 Experimental Section

2.4.1 Materials

$Re(CO)_5Cl$ and triphenylphosphine were purchased from Strem Chemicals Inc. Nitrogen was purchased from AirGas Inc. The 2–dicyclohexylphosphino–2′,6′–dimethoxybiphenyl was purchased from Sigma-Aldrich. The 2,6-dibromo-pyridine and pyridine were purchased from Alfa Aesar. The bis(dibenzylideneacetone)palladium, $Pd(dba)_2$, was purchased from Tokyo Chemical Industry Co., LTD. The 8-quinoline boronic acid was purchased from Frontier Scientific. Dried solvents (THF and toluene) were distilled over sodium/benzophenone and acetonitrile was distilled over calcium hydride.[54] The other solvents (dichloromethane, 1,2-dichlorobenzene, diethyl ether, and pentane) were used as received from the distributor.

2.4.2 Instrumentation

A PerkinElmer Spectrum 400 FT-IR/FT-FIR spectrometer was used for IR spectra taken in NaCl IR cell. A Bruker AVANCE 500 MHz NMR spectrometer was used to record NMR spectra. Absorption measurements were performed in a Varian Cary 50 Bio UV-Visible Spectrophotometer. Emission was analyzed with a Varian Cary Eclipse Fluorescence Spectrophotometer. Mass spectroscopy was performed on an Electrospray Ionization (ESI) with an Agilent Time-of-

Flight MS G1969A Series 6200 in positive ionization mode using 1 ppm of the complexes in a 50% methanol/water (LC/MS) with 10 μM of acetic acid (ionization agent).

2.4.3 Synthesis of 2,6-Bis(8'-Quinolinyl)Pyridine

An oven-dried flask was charged with 8-quinolineboronic acid (0.413 g, 2.39 mmol), 2,6-dibromo-pyridine (0.265 g, 1.12 mmol), $Pd(dba)_2$ (0.013 g, 0.023 mmol), 2–dicyclohexylphosphino–2′,6′–dimethoxybiphenyl (0.019 g, 0.046 mmol) and ground K_3PO_4 (2.27 g, 10.7 mmol). The flask was evacuated and charged with N_2. Dry toluene (10 mL) was added via a syringe and the resulting suspension was stirred at 100°C for 15 hours. The mixture was allowed to cool to room temperature, diluted with CH_2Cl_2 (30 mL) and filtered. The solvent was removed and dissolved in a minimum of CH_2Cl_2 (3 mL); the resulting solution was clear yellow. Cold hexane was added to the solution while slowly stirring, until an off-white precipitate started to appear. The mixture was placed in the freezer overnight and the solid collected via filtration. ^1H NMR (500 MHz, CD_2Cl_2): δ 8.97 (dd, 2H, *J* = 4.1, 1.9 Hz), 8.26 (m, 4H), 8.12 (d, 2H, *J* = 7.8 Hz), 7.92 (m, 3H), 7.68 (dd, 2H, *J* = 8.2, 7.2 Hz), 7.48 (dd, 2H, *J* = 8.3, 4.1 Hz).

*2.4.4 Synthesis of fac-Re(bqp-κ²N)(CO)₃Cl (**1**)*

A 300 mL round bottom flask, was charged with $Re(CO)_5Cl$ (0.1068 g,

0.295 mmol) and 2,6-bis(8′-quinolinyl)-pyridine (0.1146 g, 0.344 mmol); both are white powders. The flask was sealed with a rubber septum. Toluene (100 mL) was added via syringe and the powders dissolved. A condenser was attached and mixture brought to a reflux for 6 hours. The clear mixture turned slightly yellow as reaction progressed. The solution was allowed to cool and approximately half of the solvent removed under reduced pressure. The resulting yellow solid was filtered via Büchner funnel and put in a vial and placed under vacuum for further drying. The filtrate was collected and stored in the freezer overnight. The solvent was removed from the yellow solution via reduced vacuum filtration. The yellow residue was reprecipitated from CH_2Cl_2 using pentane. ^{1}H NMR (500 MHz, CD_2Cl_2): δ 9.68 (dd, 2H, *J* = 5.0, 1.6 Hz), 8.69 (dd, 4H, *J* = 8.2, 1.5 Hz), 8.55 (dd, 2H, *J* = 7.2, 1.4 Hz), 8.25 (m, 3H), 7.98 (dd, 2H, *J* = 8.1, 7.4 Hz), 7.90 (m, 2H). IR (CH_3CN): ν (CO) = 1902, and 2020 cm^{-1}. TOF-MS: m/z 604.0647.

*2.4.5 Synthesis of fac-[Re(bqp-κ²N)(CO)₃(NCCH₃)][CF₃SO₃] (**2**)*

A 100 mL round bottom flask was charged with *fac*-Re(bqp-κ²*N*)$(CO)_3$Cl (0.1974 g; 0.309 mmol), $AgSO_3CF_3$ (0.0821 g; 0.319 mmol), and a stir bar. The system was purged with N_2 and HPLC grade acetonitrile (50 mL) was added. A water condenser was fitted and water started. While stirring, the mixture was

brought to reflux. After 6 hours, the solution was allowed to cool to room temperature. The solution was then decanted into a celite column (3 cm x 2.5 cm) leaving much of the white AgCl behind. The flask and column were both rinsed with acetonitrile twice. The solvent was then reduced to a minimal volume for the yellow filtrate. By reprecipitating with cold diethyl ether, a yellow solid was produced and filtered. ^{1}H NMR (500 MHz, CD_2Cl_2): δ 9.87 (dd, 2H, *J* = 5.2, 1.6 Hz), 8.65 (dd, 4H, *J* = 8.2, 1.6 Hz), 8.54 (dd, 2H, *J* = 7.3, 1.4 Hz), 8.23 (m, 3H), 7.97 (m, 2H), 7.87 (d, 2H, *J* = 8.1 Hz), 2.54 (d, 2H, *J* = 11.3 Hz), 2.47 (m, 1H). IR (CH_3CN): ν (CO) = 1918, and 2028 cm^{-1}. TOF-MS: m/z 604.0647.

*2.4.6 Synthesis of fac-[Re(bqp-κ²N)(CO)₃(NC₅H₅)][CF₃SO₃] (**3**)*

A 100 mL round bottom flask was charged with *fac*-[Re(bqp-κ²*N*)(CO)$_3$(NCCH$_3$)][CF_3SO_3] (0.072 g; 0.0907 mmol), pyridine (0.21 mL, 2.596 mmol), and a stir bar. The materials were dissolved in dry THF (50 mL) and the flask was capped with a water condenser. The system was purged with N_2 for 10 minutes. The yellow solution was refluxed for four hours. After cooling to room temperature, a yellow precipitate was observed in the flask. The solid was filtered and stored in a vacuum desiccator overnight; the filtrate was left in the fume hood. The filtrate was concentrated via reduced vacuum and a yellow solid was precipitated by adding cold pentane. The yellow solid was filtered and

stored in a vacuum desiccator overnight. ^{1}H NMR (500 MHz, CD_2Cl_2): δ 9.87 (dd, 2H, *J* = 5.2, 1.6 Hz), 8.65 (dd, 4H, *J* = 8.2, 1.6 Hz), 8.54 (dd, 2H, *J* = 7.3, 1.4 Hz), 8.23 (m, 3H), 7.97 (m, 2H), 7.87 (d, 2H, *J* = 8.1 Hz). IR (CH_3CN): ν (CO) = 1919 and 2028 cm^{-1}. TOF-MS: m/z 604.0647.

*2.4.7 Synthesis of fac-[Re(bqp-κ²N)(CO)₃(PPh₃)][CF₃SO₃] (**4**)*

A 100 mL round bottom flask was charged with *fac*-[Re(bqp-κ²*N*)(CO)$_3$(NCCH$_3$)][CF_3SO_3] (0.0790 g; 0.0995 mmol), triphenyl phosphine (0.8012 g, 3.055 mmol), and a stir bar. The materials were dissolved in dry THF (50 mL) and the flask was capped with a water condenser. The system was purged with N_2 for 10 minutes. The yellow solution was refluxed for four hours. After cooling to room temperature, a yellow precipitate was observed in the flask. The solid was filtered and stored in a vacuum desiccator overnight; the filtrate was left in the fume hood. The filtrate was concentrated via reduced vacuum and a yellow solid was precipitated by adding cold pentane. The yellow solid was filtered and stored in a vacuum desiccator overnight. ^{1}H NMR (500 MHz, CD_2Cl_2): δ 9.87 (dd, 2H, *J* = 5.2, 1.6 Hz), 8.65 (dd, 4H, *J* = 8.2, 1.6 Hz), 8.54 (dd, 2H, *J* = 7.3, 1.4 Hz), 8.23 (m, 3H), 7.97 (m, 2H), 7.87 (d, 2H, *J* = 8.1 Hz). IR (CH_3CN): ν (CO) = 1918, 1923, and 2028 cm^{-1}. TOF-MS: m/z 604.0647.

CHAPTER 3.

PHOTOCHEMISTRY OF CYCLOPENTADIENYL TRICARBONYL MOLYBDENUM WITH ARENE DISULFIDES

3.1 Photochemistry of Metal-Metal Bonded Compounds

The main result of photoexcitation of metal-metal bonded complexes is homolysis[55] of the M-M bond. However, this does not detract from other possible pathways. These include one-electron oxidation,[56] halogen abstraction,[4] radical coupling,[4,57,58] radical trapping,[4b] and ligand substitution.[59]

The photochemistry of Group VI dimers, $[(\eta^5\text{-}C_5H_5)M(CO)_3]_2$ (M = Cr, Mo, W) has been heavily studied.[3,60-63] Metal dimers of tungsten and molybdenum have shown mechanisms of CO-loss and homolytic dimer cleavage intermediates through flash photolysis.[62]

The tungsten dimer, $[(\eta^5\text{-}C_5H_5)W(CO)_3]_2$, has been investigated as a possible catalyst for desulfurization of fuel stocks. Its photoreaction with disulfides has also been investigated.[63-65] However, the research of the molybdenum analog is not as well pioneered. Davidson and Sharp[3] investigated metal trifluoromethylthio-derivatives of many transition metals. They showed that reactions were possible with photolysis of the disulfides and low oxidation

state metal complexes of the nature, $[(\eta^5\text{-}C_5H_5)M(CO)_3]_2$ (M = Mo, W) and $M(CO)_5$ (M = Fe).

3.2 Results and Discussion

This is a study of the photoreaction of the molybdenum dimer, $[Cp(CO)_3Mo]_2$, with a variety of arene disulfides. It is an extension of the work done by Daniel Weinmann for his dissertation[64], where he studied the photoreaction of the analogous $[Cp(CO)_3W]_2$ with disulfides and thiols. Watkins and George[60] also have prepared some of the projected products of my work by thermal routes and IR and ^{1}H-NMR spectroscopic values were compared with their results.

3.2.1 Photoreaction of $[Cp(CO)_3Mo]_2$ and (p-tolylS)$_2$

My project began with the reaction as follows:

$$[Cp(CO)_3Mo]_2 + [(p\text{-tolyl})S]_2 + h\nu \rightarrow 2\,[Cp(CO)_3MoS(p\text{-tolyl})] \qquad (1)$$

Not all starting metal dimer was consumed with extended 60W visible light irradiation of 40 hours. Therefore, a column separation was needed in order to isolate the product. An initial adsorption column of alumina in a disposable pipet showed good separation, but a larger column size provided less separation. The target product of $Cp(CO)_3MoS(p\text{-tolyl})$, was identified by IR and ^{1}H-NMR spectroscopies. Initial comparison of NMR data with those of Watkins and George showed similar peaks at 5.26 ppm for the cyclopentadienyl ligand

and 7.88 ppm for the tolyl ligand.[60] As seen in Appendix A, the proton NMR shows two singlet peaks (4.78 and 5.05 ppm). The first peak is presumably generated by the cyclopentadienyl rings of the target product, $Cp(CO)_3MoS(p\text{-tolyl})$. The singlet at 5.05 ppm is presumed to be caused by the Cp ring of an easily formed dimer, $[Cp(CO)_3MoS(p\text{-tolyl})]_2$. Weinmann and Abrahamson[66] saw a similar result from a tungsten analog.

3.2.2 Photoreaction of $[Cp(CO)_3Mo]_2$ and $(2\text{-pyS})_2$

Due to poor column separation of the tolyl compound above, the disulfide was altered to study its reactivity. The choice was for 2,2'-dipyridyl disulfide for replacement in the reaction, as shown in equation 2.

$$[Cp(CO)_3Mo]_2 + [(2\text{-py})S]_2 + h\nu \rightarrow 2\ Cp(CO)_3MoS(2\text{-py}) \qquad (2)$$

Irradiation of the reaction mixture was done with a 60 W desk lamp or broadband UV light. The desk lamp took an extended period of irradiation (29 hours) to achieve appreciable conversion, but the UV light was found to convert 90% of the metal dimer, as monitored by is IR band at 2011 cm^{-1}, in 3–4 hours of irradiation. The reaction was monitored with IR spectroscopy for peaks as shown in Table 8. After reaction, the mixture was evaporated via dynamic vacuum.

Table 8. IR Stretching for Mo(0) Complexes

Compound	IR Stretch (cm^{-1})
$[CpMo(CO)_3]_2$	2015; 1956; 1912
$CpMo(CO)_3Spy$	2037; 1960; 1873

The mixture was dissolved in 75:25 hexane/toluene solvent and introduced onto an alumina adsorption column. The molybdenum dimer was eluted off as a purple band along with unreacted disulfide. The product was eluted with toluene as an orange band and classified with ^{1}H-NMR techniques, as shown in Table 9.

While the tricarbonyl $Cp(CO)_3MoS(2\text{-py})$ was the expected product complex based on the analogous tungsten chemistry,[63] it was suggested by IR frequencies in the carbonyl range that the dicarbonyl compound was readily formed with carbonyl loss. The dicarbonyl complex was then considered since its stability seemed adequate with the nitrogen of the pyridyl ligand presumably taking up the available coordination site formed on loss of CO, as in the analogous tungsten case.[63] The UV-vis spectroscopy was used to monitor the quantitative photochemistry and the wavelengths of interest are presented in Table 10. The quantum yield of appearance was 1.95, averaged from five trials.

Table 9. NMR Data of Mo(0) complexes and disulfides

	Proton				
	Aromatic				Cp
$(Spy)_2$	8.16, m	7.37, dd, (J = 8.2, 1.0 Hz)	6.77, td, (J = 7.8, 1.9 Hz)	6.34, ddd, (J = 7.4, 4.7, 1.0 Hz)	
$(CpMo(CO)_3)_2$					4.68, s
$CpMo(CO)_2Spy$	7.39, dt, (J = 5.6, 1.3 Hz)	6.50, ddd, (J = 8.7, 7.4, 1.6 Hz)	6.27, dt, (J = 8.4, 1.1 Hz)	5.98, ddd, (J = 7.0, 5.7, 1.2 Hz)	
$CpMo(CO)_3Stolyl$					4.78, s

Table 10. Molar extinction coefficients (ε, M^{-1} cm^{-1})

Wavelength (nm)	366	390[a]	417[b]	512[a]	546
$[CpMo(CO)_3]_2$	6513	20213	5373	1965	1597
$[CpMo(CO)_2S(py)$	2235	3216	4019	485	307

[a] Peaks made by metal dimer. [b] Peak made by product.

3.3 Experimental Section

3.3.1 Materials

All materials were used as received unless otherwise stated. Molybdenum dimer was purchased from Sigma Aldrich Co. Pre-purified nitrogen was purchased from AirGas Co. and passed through oxygen scrubbing and drying columns before entering the system. All NMR spectra were taken in C_6D_6 purchased from Sigma Aldrich Co.

3.3.2 Instrumentation

A PerkinElmer Spectrum 400 FT-IR/FT-FIR spectrometer was used for IR spectra taken in an NaCl IR cell sealed with serum caps. An ordinary 60-watt desk lamp was used for visible light irradiation. A Bruker AVANCE 500 MHz NMR spectrometer was used to record NMR spectra. Extinction coefficient measurements were performed using a Shimadzu UV-2501PC UV-Vis Recording Spectrometer in a quartz "H cell" cuvette for inert atmosphere.

3.3.3 Synthesis of $Cp(CO)_3MoS(p\text{-tolyl})$

A nitrogen-purged THF solution of 0.300 g of $[Cp(CO)_3Mo]_2$ and 0.308 g $[(p\text{-tolyl})S]_2$ was made in a two neck 50 mL round bottom flask with a gas inlet. The resulting purple mixture was irradiated with visible light from a 60 W desk lamp for one hour and an IR spectrum was taken. Only starting material was seen, so the irradiation was continued for 20 hours. A slight orange color was

present with some orange residue. The mixture was irradiated for an additional 20 hours but no further change was apparent by IR spectroscopy.

A column separation was attempted with a pipet filled with alumina adsorption powder. A 1–2 mL portion of the reaction mixture was introduced to the column and starting material was separated with toluene elution. It was visible as a purple band, with an orange band eluting slowly behind. The orange band was then eluted with THF. The resulting solution was a transparent yellow/orange color. Proton NMR spectra showed not enough material present for characterization. In an attempt to enlarge the separation column, the elution was not as clean due to the introduction technique used.

A second attempt at the irradiation produced the same results up to the elution. Therefore, the purple solution was removed from the orange powder via cannula. The orange powder was dissolved in C_6D_6 and ^{1}H-NMR spectra were taken. A second attempt with a more concentrated sample was done.

3.3.4 Synthesis of [Cp(CO)$_2$MoS(2-pyridyl)]

Metal dimer, $[Cp(CO)_3Mo]_2$, weighing 0.330 g (0.673 mmole) was degassed and back filled with N_2 with 0.148 g (0.672 mmole) of dipyridyl disulfide in a 50 mL round bottom flask fitted with an air-free adaptor and a magnetic stirrer. The solids were allowed to dissolve in 30 mL of dried, oxygen-free THF giving a maroon colored solution; a small aliquot was removed to get a baseline IR

spectra. A 60 W desk lamp was placed 20 cm away and turned on. An IR spectrum was taken periodically to follow the reaction and irradiation was stopped after 6 hours when the Mo dimer peak at 2011 cm^{-1} was approximately 10% of the initial strength. The solution appeared to contain an orange hue. The solvent was removed via dynamic vacuum and left behind an orange powder.

An initial column of alumina adsorption was constructed using a disposable pipet. A 5 mL volume of 1:1 hexane/toluene was used to dissolve some powder and was introduced to the column. A pink/purple band of unreacted metal dimer was eluted first using 1:1 hexane/toluene. An orange band of the product slowly moved down the column and was removed with THF. The product solution was dried and IR and ^{1}H-NMR were done to determine purity. A larger 30 cm long column, 2–cm diameter 1–m long fritted glass tube, was made with hexane packed alumina adsorption and the remaining orange product was dissolved in 1:1 hexane/toluene in two 10–15 mL portions. A small pink band of metal dimer was removed first and the orange band of the product was removed with toluene. Proton NMR showed some disulfide still present, so a second column was constructed. A new solvent mixture, 75:25 hexane/toluene, was used to dissolve and elute starting material and slow down the progression of the product band. Trace amounts of disulfide were still present in an NMR spectrum. Therefore, the dried orange powder was washed

with hexane. The hexane was removed via syringe and an NMR was taken of the powder left behind and removed. This shown a majority of disulfide was removed with some product. ^{1}H NMR (500 MHz, C_6D_6): δ 7.39 (dt, 1H, *J* = 5.6, 1.3 Hz), 6.50 (ddd, 1H, *J* = 8.7, 7.4 Hz), 6.27 (dt, 1H, *J* = 8.4, 1.1 Hz), 5.98 (ddd, 1H, *J* = 7.0, 5.7, 1.2 Hz), 4.84 (s, 5H).

3.3.5 Photochemical Procedure

The irradiation source was green light with a wavelength of 546 nm produced by a medium pressure mercury arc lamp and band-pass filter. The reactions were monitored by UV-Vis spectroscopy. Quantum yields were measured in 4 mL solution of the reactants in a 1 cm cell length cuvette with an attached tube and were degassed by three freeze-pump-thaw cycles. The intensity of the light was measured by ferrioxalate actinometry using Weinmann's adaptation[64] of procedures of Hatchard and Parker.[67]

3.3.6 Quantitative Photochemistry

A solution of 0.0102 g of Mo dimer and 0.0044 g of $[S(py)]_2$ was mixed with 60 mL of dried toluene and stored in the dark. A 1.5 mL aliquot of the solution was transferred into an H-tube custom glassware and diluted with 5 mL of dried toluene. The mixture was freeze-degassed-thawed three times and irradiated with light. The first trials were irradiated with UV light for 15–30 minutes but the time scale was shorted to 5–10 minutes due to complete

conversion with the longer times. Since the initial product is the tricarbonyl, we wanted to see how long it took for the dicarbonyl to form. Therefore, trials were irradiated and measurements were taken, and the solution was allowed to rest in the dark with periodic monitoring by UV-vis spectroscopy. The transformation seemed to take place with a 24 hour resting after irradiation.

The irradiation wavelengths of 366 and 546 nm were monitored and the longer wavelength was chosen since the light source was available for immediate use. The absorption readings were then administered to a calculation for quantum yields designed by Weinmann.[64] The first calculation attempt suffered from inaccuracies due to high absorption at 390 nm, prompting a second attempt with a lowered concentration.

Appendix A

NMR spectra

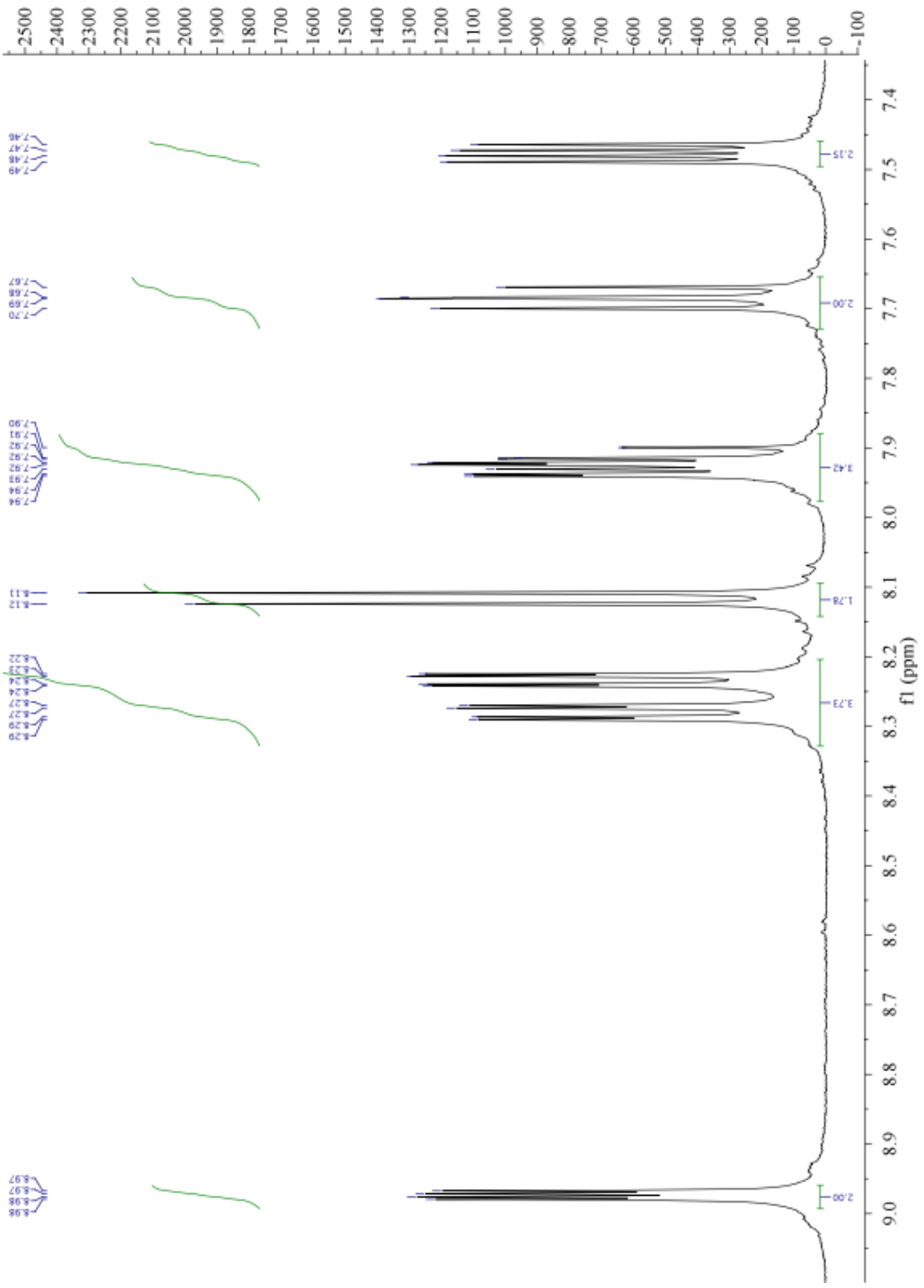

Figure 11. ^{1}H-NMR spectrum of 2,6-bis(8′-quinolinyl)pyridine. (The solvent is CD_2Cl_2)

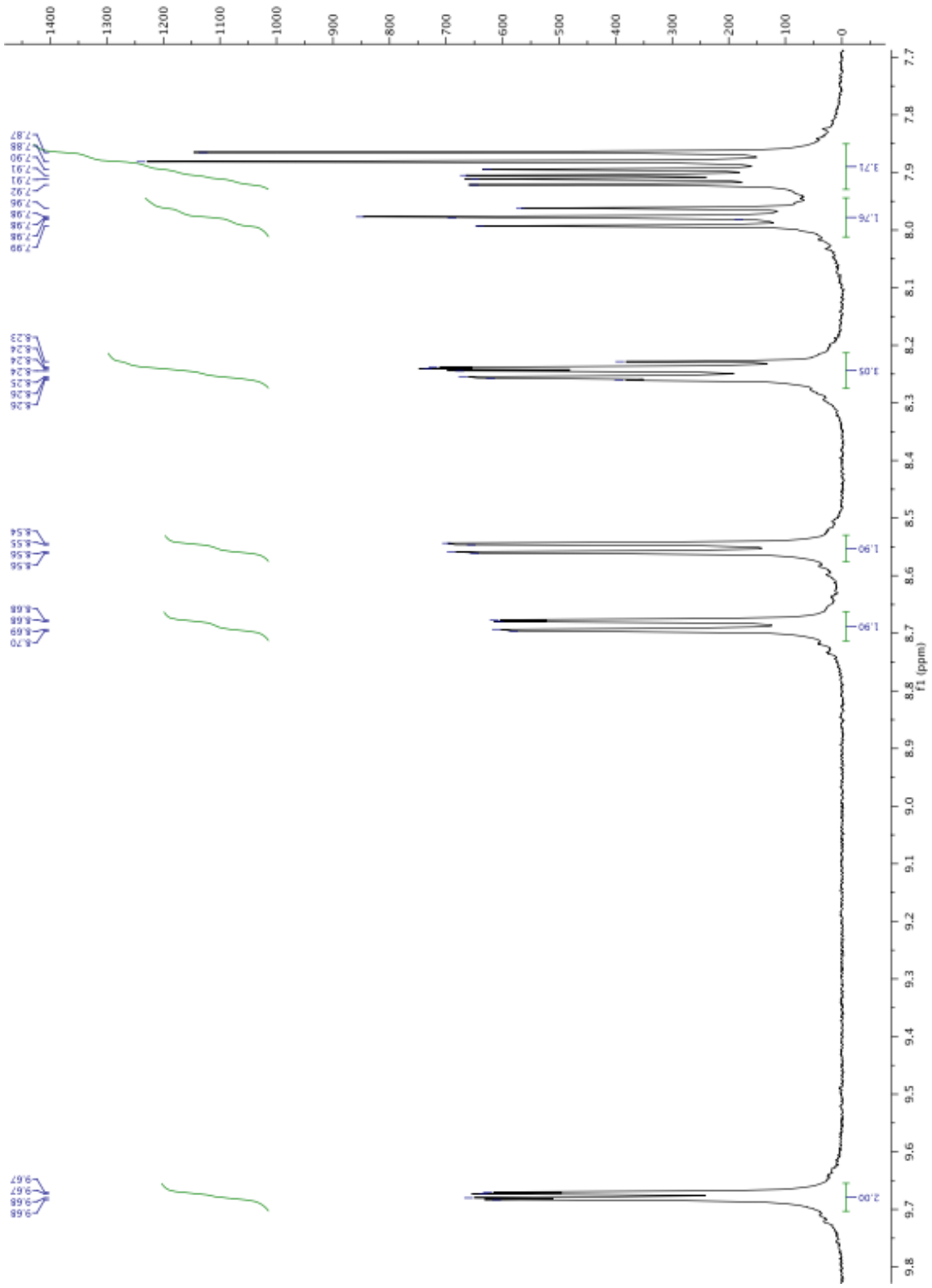

Figure 12. ^{1}H-NMR spectrum of *fac*-Re(bqp-κ^{2}*N*)(CO)$_{3}$Cl. (The solvent is CD_2Cl_2)

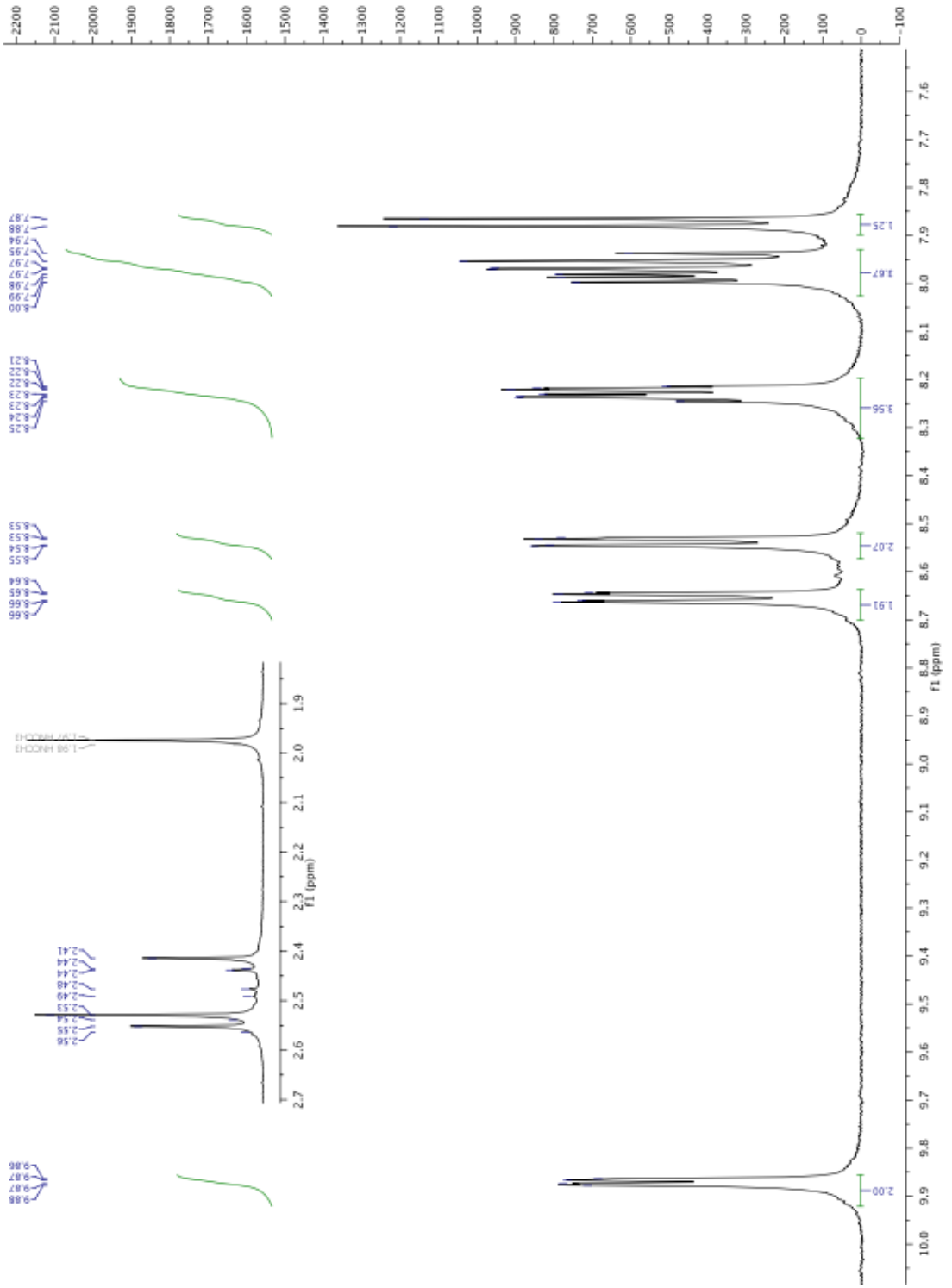

Figure 13. ^{1}H-NMR spectrum of *fac*-[Re(bqp-κ^{2}*N*)(CO)$_3$(NCCH$_3$)]$^{+}$. (The solvent is CD_2Cl_2)

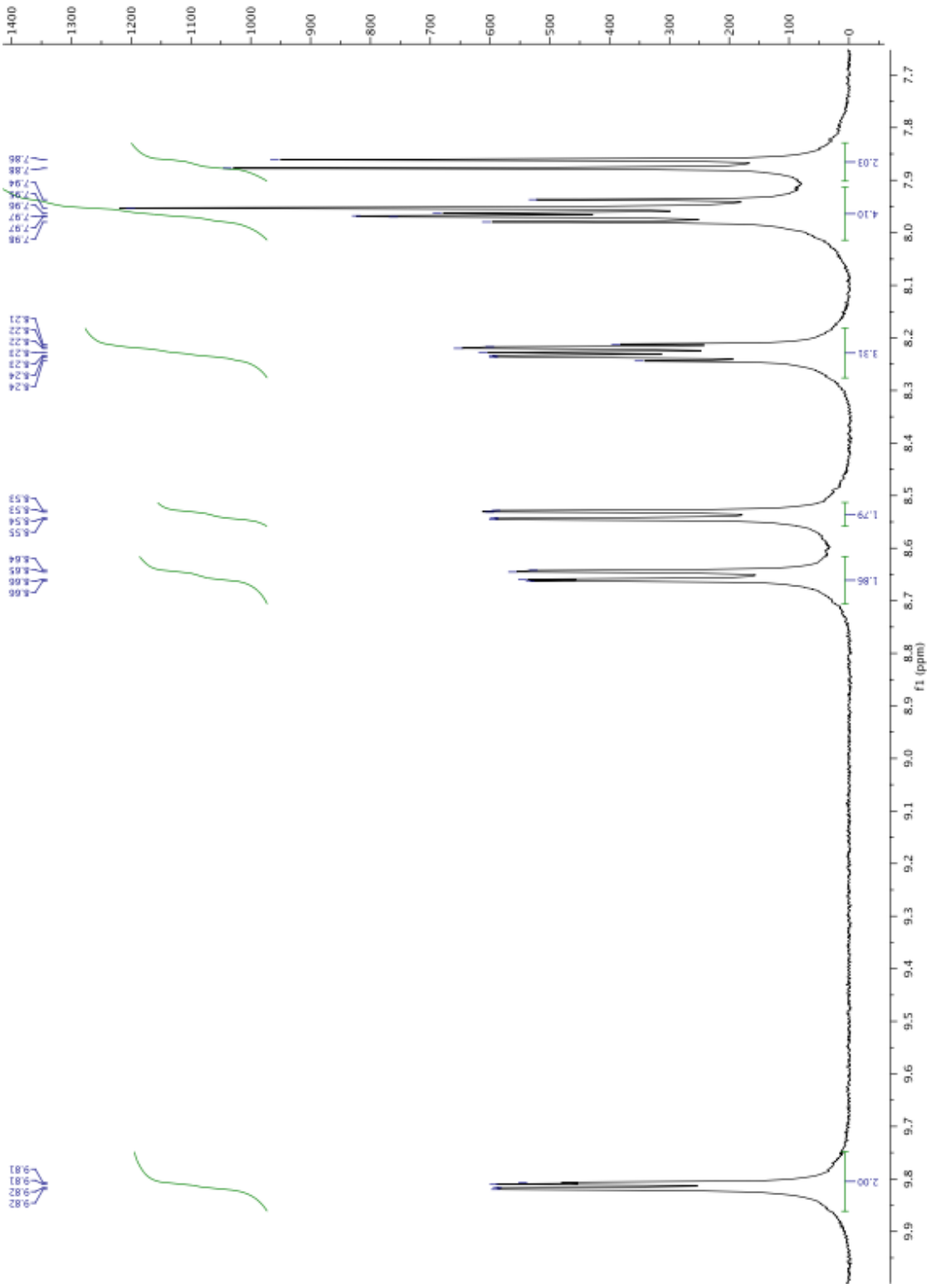

Figure 14. ^{1}H-NMR spectrum of *fac*-[Re(bqp-κ^{3}*N*)(CO)$_3$]$^+$. (The solvent is CD_2Cl_2)

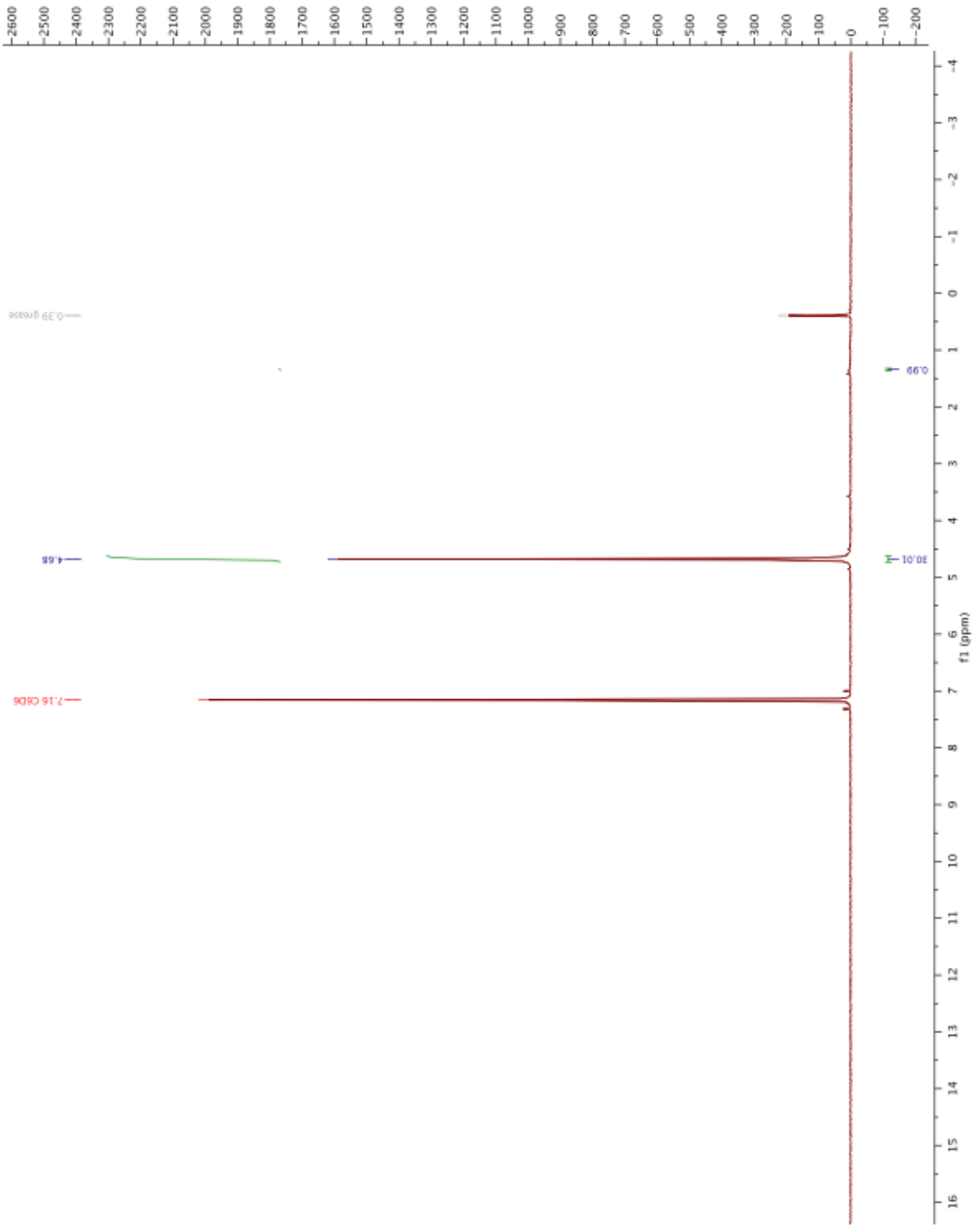

Figure 15. ^{1}H-NMR spectrum of $[(\eta^5\text{-}C_5H_5)Mo(CO)_3]_2$. (The solvent is C_6D_6)

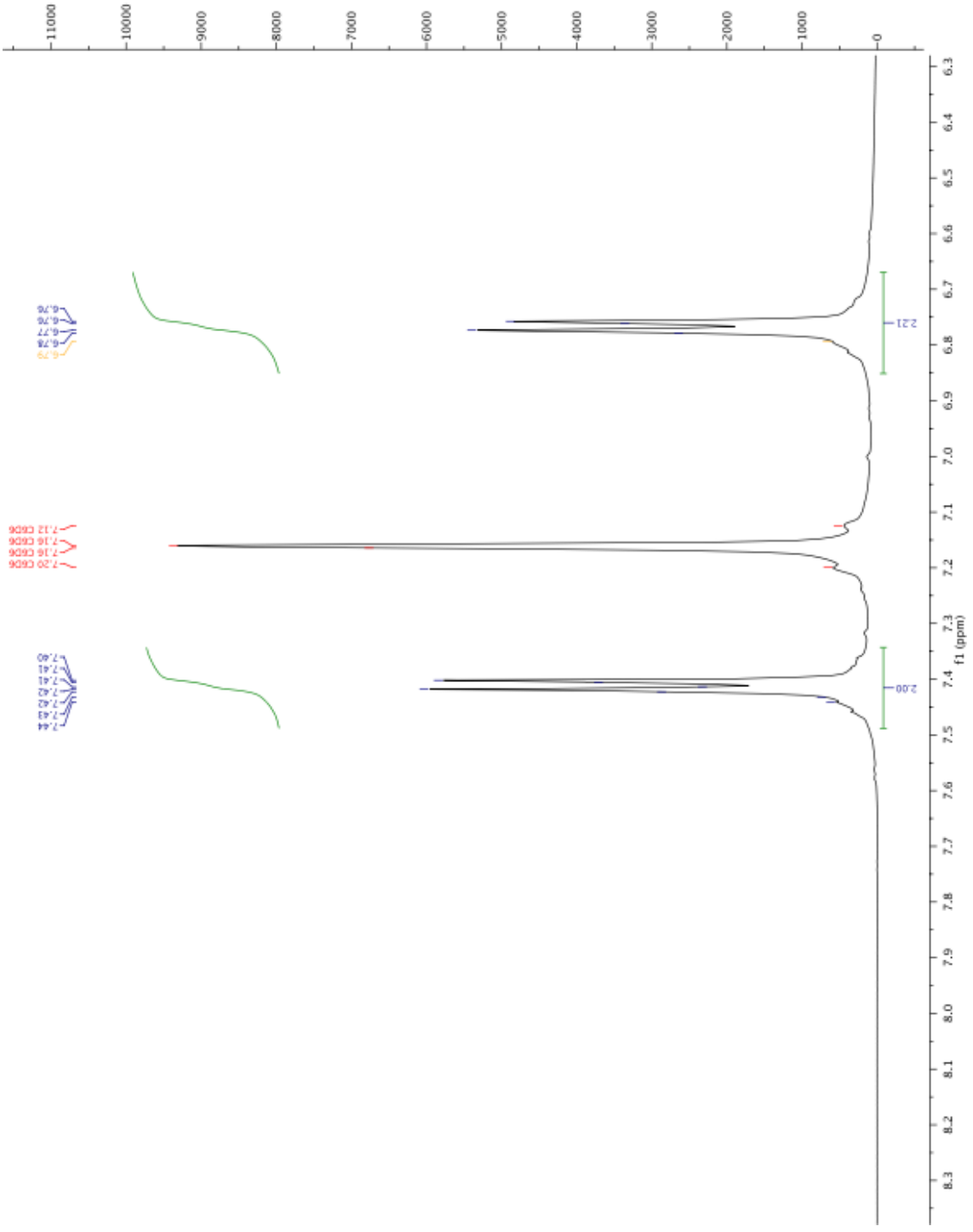

Figure 16. ^{1}H-NMR spectrum of (p-tolylS)$_2$. (The solvent is C_6D_6)

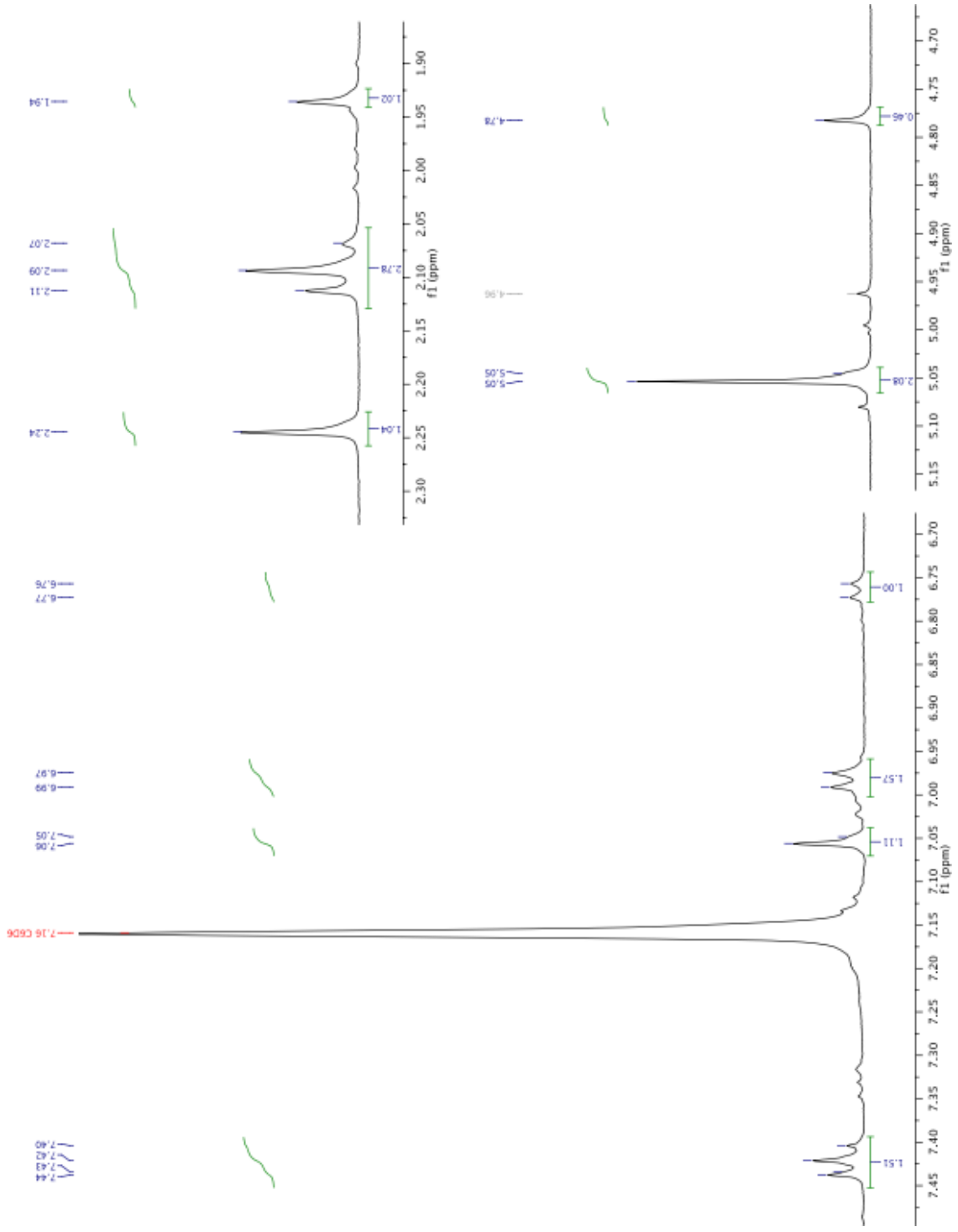

Figure 17. ^{1}H-NMR spectrum of (η^5-C_5H_5)Mo(CO)$_3$(*p*-tolylS). (The solvent is C_6D_6)

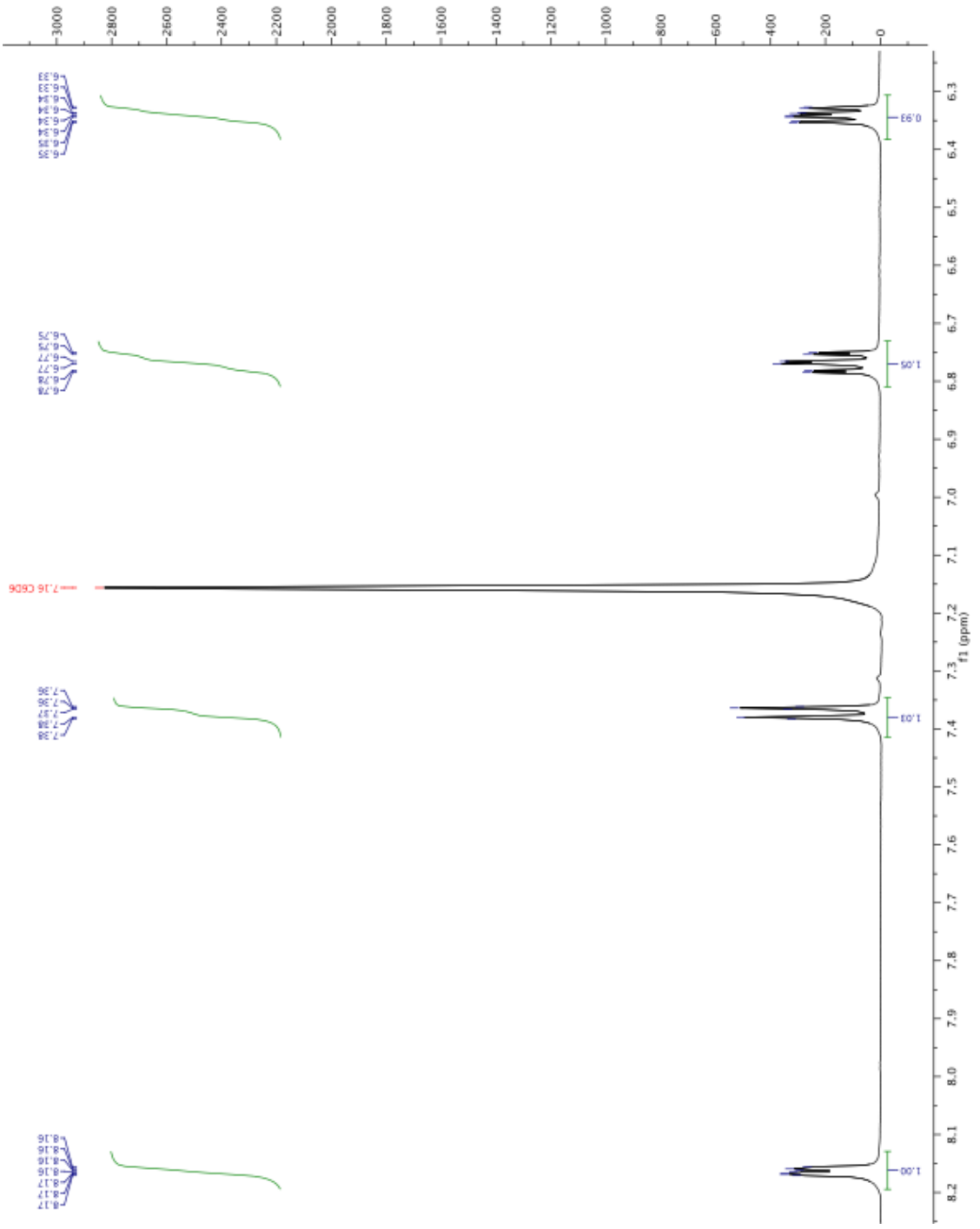

Figure 18. ^{1}H-NMR spectrum of $(2\text{-pyS})_2$. (The solvent is C_6D_6)

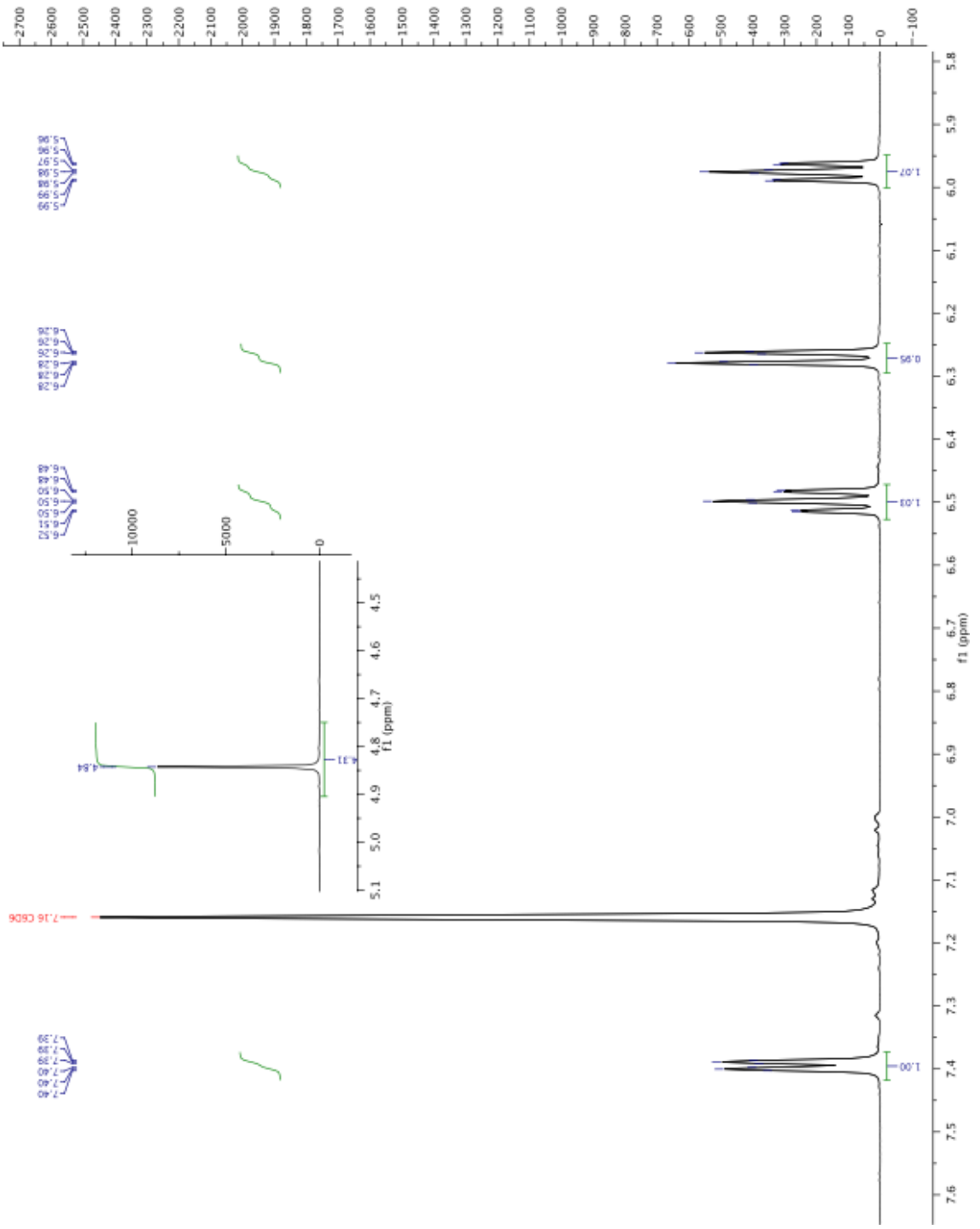

Figure 19. ^{1}H-NMR spectrum of (η^5-C_5H_5)Mo(CO)$_2$(2-pyS). (The solvent is C_6D_6)

Appendix B

Excited States of Bisquinolinyl Pyridine Rhenium(I) Complexes

Calculated singlet excited-states of *fac*-Re(bqp-κ^2*N*)$(CO)_3Cl$ in CH_3CN. The excited state number is followed by the spin multiplicity, symmetry, excitation energy, and oscillator strength *f*. The excitations from occupied to virtual orbitals are listed on the next line, followed by the wavefunction coefficients.

Excited State 1: Singlet-A 3.0297 eV 409.23 nm f=0.0110 <S**2>=0.000
123 ->125 -0.11145
124 ->125 0.69110
This state for optimization and/or second-order correction.
Total Energy, E(TD-HF/TD-KS) = -1929.10885832
Copying the excited state density for this state as the 1-particle RhoCI density.

Excited State 2: Singlet-A 3.1508 eV 393.50 nm f=0.0102 <S**2>=0.000
122 ->125 -0.37460
123 ->125 0.59427

Excited State 3: Singlet-A 3.2835 eV 377.59 nm f=0.0843 <S**2>=0.000
120 ->125 0.10832
122 ->125 0.57808
123 ->125 0.35141
124 ->125 0.12106

Excited State 4: Singlet-A 3.6949 eV 335.55 nm f=0.0410 <S**2>=0.000
121 ->125 0.68483

Excited State 5: Singlet-A 3.7517 eV 330.48 nm f=0.0215 <S**2>=0.000
124 ->126 0.64458
124 ->127 -0.26229

Excited State 6: Singlet-A 3.8517 eV 321.89 nm f=0.0152 <S**2>=0.000
120 ->125 0.38155
122 ->126 -0.14445
123 ->126 0.48268
123 ->127 -0.27270

Excited State 7: Singlet-A 3.8911 eV 318.64 nm f=0.1025 <S**2>=0.000
120 ->125 0.52626
122 ->126 0.27550
122 ->127 -0.14319
123 ->126 -0.30205

Excited State 8: Singlet-A 3.9326 eV 315.28 nm f=0.0130 <S**2>=0.000
120 ->125 0.13651
122 ->126 -0.39709
122 ->127 0.16675
123 ->126 -0.15615
124 ->126 0.17545
124 ->127 0.44636

Excited State 9: Singlet-A 3.9599 eV 313.10 nm f=0.0278 <S**2>=0.000
120 ->125 -0.11705
122 ->126 0.31728
122 ->127 -0.24907
123 ->126 0.20452
124 ->126 0.18443
124 ->127 0.46798

Excited State 10: Singlet-A 4.0500 eV 306.13 nm f=0.0067 <S**2>=0.000
122 ->127 -0.11690
123 ->126 0.26402
123 ->127 0.62069

Excited State 11: Singlet-A 4.0710 eV 304.55 nm f=0.0035 <S**2>=0.000
122 ->127 0.25999
124 ->128 0.32488
124 ->129 0.35958
124 ->130 0.34103
124 ->132 0.10835

Excited State 12: Singlet-A 4.1277 eV 300.37 nm f=0.0316 <S**2>=0.000
119 ->125 -0.25860
122 ->126 0.30723
122 ->127 0.50384
123 ->126 0.10550
124 ->129 -0.13870
124 ->130 -0.10461

Calculated singlet excited-states of *fac*-[Re(bqp-κ²*N*)(CO)₃(NCCH₃)]⁺ in CH₃CN. The excited state number is followed by the spin multiplicity, symmetry, excitation energy, and oscillator strength *f*. The excitations from occupied to virtual orbitals are listed on the next line, followed by the wavefunction coefficients.

Excited State 1: Singlet-A 3.3311 eV 372.20 nm f=0.1140 <S**2>=0.000
126 ->127 0.68572
This state for optimization and/or second-order correction.
Total Energy, E(TD-HF/TD-KS) = -1601.48607223
Copying the excited state density for this state as the 1-particle RhoCI density.

Excited State 2: Singlet-A 3.4738 eV 356.91 nm f=0.0085 <S**2>=0.000
124 ->127 0.55081
125 ->127 -0.42482

Excited State 3: Singlet-A 3.5985 eV 344.54 nm f=0.0101 <S**2>=0.000
123 ->127 0.62325
124 ->127 -0.25329
125 ->127 -0.19395

Excited State 4: Singlet-A 3.7032 eV 334.80 nm f=0.0792 <S**2>=0.000
123 ->127 0.30715
124 ->127 0.34095
125 ->127 0.51707

Excited State 5: Singlet-A 3.9016 eV 317.77 nm f=0.0469 <S**2>=0.000
121 ->127 -0.13922
122 ->127 0.62330
126 ->128 0.19631
126 ->129 -0.14124

Excited State 6: Singlet-A 3.9608 eV 313.03 nm f=0.0450 <S**2>=0.000
122 ->127 -0.23125
126 ->128 0.56778
126 ->129 -0.27246

Excited State 7: Singlet-A 4.1209 eV 300.86 nm f=0.0016 <S**2>=0.000
121 ->127 0.67930
122 ->127 0.13571

Calculated singlet excited-states of *fac*-[Re(bqp-κ²*N*)(CO)$_3$(NC$_5$H$_5$)]$^+$ in CH$_3$CN. The excited state number is followed by the spin multiplicity, symmetry, excitation energy, and oscillator strength *f*. The excitations from occupied to virtual orbitals are listed on the next line, followed by the wavefunction coefficients.

Excited State 1: Singlet-A 3.2643 eV 379.82 nm f=0.0870 <S**2>=0.000
134 ->137 0.10087
135 ->137 0.24701
136 ->137 0.64420
This state for optimization and/or second-order correction.
Total Energy, E(TD-HF/TD-KS) = -1717.02116870
Copying the excited state density for this state as the 1-particle RhoCI density.

Excited State 2: Singlet-A 3.3572 eV 369.30 nm f=0.0334 <S**2>=0.000
135 ->137 0.65663
136 ->137 -0.23951

Excited State 3: Singlet-A 3.5474 eV 349.50 nm f=0.0072 <S**2>=0.000
133 ->137 0.64375
134 ->137 0.27460

Excited State 4: Singlet-A 3.6755 eV 337.32 nm f=0.0620 <S**2>=0.000
133 ->137 -0.27561
134 ->137 0.63027

Excited State 5: Singlet-A 3.8477 eV 322.23 nm f=0.0163 <S**2>=0.000
132 ->137 0.47928
136 ->138 -0.44366
136 ->139 -0.12990
136 ->140 -0.14655

Excited State 6: Singlet-A 3.8799 eV 319.55 nm f=0.1051 <S**2>=0.000
132 ->137 0.47933
136 ->138 0.44787
136 ->140 0.10950

Excited State 7: Singlet-A 4.0038 eV 309.67 nm f=0.0106 <S**2>=0.000
136 ->139 0.66285
136 ->140 -0.12110

Excited State 8: Singlet-A 4.0412 eV 306.80 nm f=0.0253 <S**2>=0.000
135 ->138 0.65362
135 ->140 0.14435
135 ->143 -0.10188

Excited State 9: Singlet-A 4.0869 eV 303.37 nm f=0.0010 <S**2>=0.000
131 ->137 0.69476

Excited State 10: Singlet-A 4.1562 eV 298.31 nm f=0.0104 <S**2>=0.000
133 ->138 0.56231
133 ->140 0.18728
133 ->145 -0.12165
134 ->138 0.25572
135 ->139 -0.12580

Excited State 11: Singlet-A 4.1745 eV 297.00 nm f=0.0264 <S**2>=0.000
136 ->138 -0.19499
136 ->140 0.64237

Excited State 12: Singlet-A 4.2030 eV 294.99 nm f=0.0032 <S**2>=0.000
130 ->137 0.66292

Excited State 13: Singlet-A 4.2161 eV 294.08 nm f=0.0400 <S**2>=0.000
129 ->137 -0.10682
130 ->137 0.14852
133 ->138 0.11459
133 ->139 -0.11846
135 ->139 0.60314
136 ->142 0.11675

Excited State 14: Singlet-A 4.2353 eV 292.74 nm f=0.0299 <S**2>=0.000
129 ->137 0.33939
134 ->138 -0.25712
134 ->139 -0.18166
134 ->142 -0.16456
136 ->141 -0.28244
136 ->142 -0.31628
136 ->143 0.10510

Excited State 15: Singlet-A 4.2407 eV 292.37 nm f=0.0411 <S**2>=0.000

129 ->137	0.23529
133 ->138	-0.18020
134 ->138	0.45110
134 ->139	0.17495
135 ->139	0.20596
136 ->138	-0.13776
136 ->142	-0.20184

Calculated singlet excited-states of *fac*-[Re(bqp-κ²*N*)(CO)₃(PPh₃)]⁺ in CH_3CN. The excited state number is followed by the spin multiplicity, symmetry, excitation energy, and oscillator strength *f*. The excitations from occupied to virtual orbitals are listed on the next line, followed by the wavefunction coefficients.

Excited State 1: Singlet-A 3.4068 eV 363.93 nm f=0.0664 <S**2>=0.000
183 ->185 0.12420
184 ->185 0.67844
This state for optimization and/or second-order correction.
Total Energy, E(TD-HF/TD-KS) = -2505.00415752
Copying the excited state density for this state as the 1-particle RhoCI density.

Excited State 2: Singlet-A 3.5717 eV 347.13 nm f=0.0033 <S**2>=0.000
181 ->185 -0.30088
182 ->185 0.62325
183 ->185 0.10751

Excited State 3: Singlet-A 3.6141 eV 343.05 nm f=0.1044 <S**2>=0.000
180 ->185 0.14037
181 ->185 0.23767
183 ->185 0.62419
184 ->185 -0.11663

Excited State 4: Singlet-A 3.6671 eV 338.10 nm f=0.0484 <S**2>=0.000
180 ->185 0.32081
181 ->185 0.48059
182 ->185 0.28787
183 ->185 -0.25716

Excited State 5: Singlet-A 3.8743 eV 320.02 nm f=0.0125 <S**2>=0.000
177 ->185 0.12534
178 ->185 0.10100
179 ->185 0.11895
180 ->185 0.54929
181 ->185 -0.32011
182 ->185 -0.13577
184 ->186 -0.11879

Excited State 6: Singlet-A 3.9069 eV 317.35 nm f=0.0405 <S**2>=0.000
180 ->185 0.11735
183 ->186 0.18226
184 ->186 0.62368
184 ->187 0.15596

Excited State 7: Singlet-A 4.0029 eV 309.73 nm f=0.0288 <S**2>=0.000
174 ->185 0.13601
176 ->185 0.12269
177 ->185 0.11340
178 ->185 0.59930
179 ->185 -0.17621
183 ->186 0.11516

Excited State 8: Singlet-A 4.0720 eV 304.48 nm f=0.0378 <S**2>=0.000
179 ->185 0.46881
180 ->185 -0.11492
183 ->186 0.43753
184 ->186 -0.12908

Excited State 9: Singlet-A 4.0827 eV 303.68 nm f=0.0688 <S**2>=0.000
177 ->185 -0.15199
178 ->185 -0.15047
179 ->185 -0.41507
180 ->185 0.14795
182 ->186 0.14358
183 ->186 0.41609
184 ->186 -0.14225

Excited State 10: Singlet-A 4.1326 eV 300.01 nm f=0.0078 <S**2>=0.000
175 ->185 0.19777
176 ->185 0.35817
177 ->185 0.46395
178 ->185 -0.15773
179 ->185 -0.11482
182 ->186 -0.17763

Excited State 11: Singlet-A 4.1488 eV 298.84 nm f=0.0055 <S**2>=0.000

176 ->185	0.53973
177 ->185	-0.36832
179 ->185	0.15648

Excited State 12: Singlet-A 4.1582 eV 298.17 nm f=0.0233 <S**2>=0.000

174 ->185	0.12616
175 ->185	-0.20900
176 ->185	0.10535
177 ->185	0.22464
178 ->185	-0.18046
181 ->186	-0.11522
182 ->186	0.49356
182 ->189	-0.13883
183 ->186	-0.10275
184 ->187	-0.12670

Calculated singlet excited-states of *fac*-[Re(bqp-κ^3*N*)(CO)$_3$]$^+$ in CH_3CN. The excited state number is followed by the spin multiplicity, symmetry, excitation energy, and oscillator strength *f*. The excitations from occupied to virtual orbitals are listed on the next line, followed by the wavefunction coefficients.

Excited State 1: Singlet-A 3.1381 eV 395.09 nm f=0.1678 <S**2>=0.000
112 ->116 0.15262
115 ->116 0.68029
This state for optimization and/or second-order correction.
Total Energy, E(TD-HF/TD-KS) = -1468.73564952
Copying the excited state density for this state as the 1-particle RhoCI density.

Excited State 2: Singlet-A 3.2269 eV 384.22 nm f=0.0206 <S**2>=0.000
113 ->116 0.23182
114 ->116 0.64806
115 ->117 -0.12872

Excited State 3: Singlet-A 3.2987 eV 375.86 nm f=0.0066 <S**2>=0.000
113 ->116 0.66513
114 ->116 -0.22746

Excited State 4: Singlet-A 3.4398 eV 360.44 nm f=0.0233 <S**2>=0.000
112 ->117 0.14119
114 ->116 0.13254
115 ->117 0.67268

Excited State 5: Singlet-A 3.4705 eV 357.25 nm f=0.0842 <S**2>=0.000
112 ->116 0.10777
114 ->117 0.68596

Excited State 6: Singlet-A 3.5528 eV 348.98 nm f=0.0559 <S**2>=0.000
112 ->116 0.41765
113 ->117 0.54493
114 ->117 -0.11217

Excited State 7: Singlet-A 3.5805 eV 346.28 nm f=0.1212 <S**2>=0.000
112 ->116 0.52782
113 ->117 -0.43820
115 ->116 -0.13217

Excited State 8: Singlet-A 3.8647 eV 320.81 nm f=0.0136 <S**2>=0.000
112 ->117 0.66816
115 ->117 -0.13953
115 ->118 0.12055

Excited State 9: Singlet-A 3.8651 eV 320.78 nm f=0.0020 <S**2>=0.000
112 ->117 -0.12135
112 ->118 0.12887
115 ->118 0.66418

Excited State 10: Singlet-A 3.9666 eV 312.57 nm f=0.0005 <S**2>=0.000
111 ->116 0.11051
113 ->118 0.11142
114 ->118 0.66644
114 ->122 0.10049

Excited State 11: Singlet-A 4.0881 eV 303.28 nm f=0.0121 <S**2>=0.000
111 ->116 0.61447
113 ->118 -0.26533
115 ->119 0.13992

Excited State 12: Singlet-A 4.1227 eV 300.73 nm f=0.0357 <S**2>=0.000
111 ->116 0.25956
112 ->119 -0.18445
113 ->118 0.50155
114 ->118 -0.10980
115 ->119 -0.28728
115 ->123 -0.11524

Calculated triplet excited-states of *fac*-Re(bqp-κ²*N*)(CO)₃Cl in CH_3CN. The excited state number is followed by the spin multiplicity, symmetry, excitation energy, and oscillator strength *f*. The excitations from occupied to virtual orbitals are listed on the next line, followed by the wavefunction coefficients.

Excited State 1: Triplet-A 2.4940 eV 497.14 nm f=0.0000 <S**2>=2.000
114 ->125 -0.12444
119 ->125 -0.12368
120 ->125 -0.27482
121 ->125 0.33342
122 ->125 0.32415
123 ->125 0.27274
124 ->125 0.21292
This state for optimization and/or second-order correction.
Total Energy, E(TD-HF/TD-KS) = -1929.12854653
Copying the excited state density for this state as the 1-particle RhoCI density.

Excited State 2: Triplet-A 2.7816 eV 445.73 nm f=0.0000 <S**2>=2.000
119 ->132 0.12961
121 ->126 0.41912
121 ->127 0.22608
122 ->126 -0.27657
122 ->127 -0.12975
123 ->126 -0.29007
123 ->127 -0.13547

Excited State 3: Triplet-A 2.9713 eV 417.28 nm f=0.0000 <S**2>=2.000
122 ->125 -0.14935
123 ->125 -0.11575
124 ->125 0.65123

Excited State 4: Triplet-A 3.1000 eV 399.95 nm f=0.0000 <S**2>=2.000
122 ->125 -0.39592
123 ->125 0.56814

Excited State 5: Triplet-A 3.3217 eV 373.26 nm f=0.0000 <S**2>=2.000

116 ->125	0.12356
117 ->125	0.19432
119 ->125	0.11002
120 ->125	0.40221
121 ->125	-0.13794
122 ->125	0.38801
123 ->125	0.22330

Excited State 6: Triplet-A 3.5004 eV 354.20 nm f=0.0000 <S**2>=2.000

111 ->125	-0.12233
111 ->127	-0.11734
114 ->125	0.18399
114 ->128	0.10086
116 ->125	-0.13360
120 ->128	-0.14508
121 ->126	-0.11635
121 ->127	0.12654
121 ->128	0.10793
122 ->125	0.11736
122 ->127	0.14723
123 ->126	-0.22842
123 ->127	0.30034
124 ->125	0.12542
124 ->126	0.12468

Excited State 7: Triplet-A 3.5947 eV 344.91 nm f=0.0000 <S**2>=2.000

116 ->125	0.21537
117 ->125	0.46476
121 ->125	0.26364
122 ->125	-0.18621
123 ->125	-0.12103
124 ->126	0.18912
124 ->127	-0.14178

Excited State 8: Triplet-A 3.6456 eV 340.09 nm f=0.0000 <S**2>=2.000

117 ->125	-0.28176
120 ->127	0.10658
124 ->126	0.43612
124 ->127	-0.28584
124 ->131	-0.10915

Excited State	9:	Triplet-A	3.7169 eV	333.57 nm	f=0.0000	<S**2>=2.000
114 ->125	0.10120					
116 ->125	-0.13204					
117 ->125	-0.19392					
120 ->125	0.27755					
121 ->125	0.43416					
121 ->127	0.12720					
123 ->126	0.10739					
124 ->128	-0.12829					
124 ->129	-0.10273					
124 ->130	-0.17311					

Calculated triplet excited-states of *fac*-[Re(bqp-κ²*N*)(CO)₃(NCCH₃)]⁺ in CH_3CN. The excited state number is followed by the spin multiplicity, symmetry, excitation energy, and oscillator strength *f*. The excitations from occupied to virtual orbitals are listed on the next line, followed by the wavefunction coefficients.

Excited State 1: Triplet-A 2.4995 eV 496.03 nm f=0.0000 <S**2>=2.000
118 ->127 -0.13800
120 ->127 -0.11328
122 ->127 -0.21747
124 ->127 0.10933
125 ->127 0.40858
126 ->127 0.43800
This state for optimization and/or second-order correction.
Total Energy, E(TD-HF/TD-KS) = -1601.51663250
Copying the excited state density for this state as the 1-particle RhoCI density.

Excited State 2: Triplet-A 2.7951 eV 443.58 nm f=0.0000 <S**2>=2.000
121 ->134 -0.15717
124 ->128 -0.15683
124 ->129 -0.12235
125 ->128 -0.27134
125 ->129 -0.22157
126 ->128 0.41374
126 ->129 0.29922

Excited State 3: Triplet-A 3.2842 eV 377.52 nm f=0.0000 <S**2>=2.000
122 ->127 0.26586
124 ->127 0.30150
125 ->127 -0.30361
125 ->128 0.10432
126 ->127 0.34697
126 ->130 0.10201
Excited State 4: Triplet-A 3.4072 eV 363.89 nm f=0.0000 <S**2>=2.000
119 ->127 -0.36000
122 ->127 -0.26791
123 ->127 0.19785
124 ->127 0.41394
125 ->127 -0.11442
126 ->127 -0.20202

Excited State 5: Triplet-A 3.4639 eV 357.93 nm f=0.0000 <S**2>=2.000

119 ->127	-0.24301
123 ->127	0.44697
124 ->127	-0.25114
125 ->127	-0.14416
126 ->127	0.21735

Excited State 6: Triplet-A 3.5653 eV 347.76 nm f=0.0000 <S**2>=2.000

118 ->127	-0.18711
119 ->127	0.10395
123 ->127	0.37063
124 ->127	-0.14733
125 ->127	0.17161
125 ->128	0.14723
125 ->129	-0.12719
126 ->127	-0.23318
126 ->128	0.20698
126 ->129	-0.21547

Excited State 7: Triplet-A 3.6595 eV 338.80 nm f=0.0000 <S**2>=2.000

118 ->127	0.10266
119 ->127	0.41996
123 ->127	0.23698
124 ->127	0.29134
125 ->128	-0.13836
125 ->129	0.10968
126 ->127	-0.12175

Excited State 8: Triplet-A 3.7366 eV 331.81 nm f=0.0000 <S**2>=2.000

118 ->127	0.10208
119 ->127	-0.26804
122 ->127	0.34818
123 ->127	-0.10846
124 ->127	0.14174
124 ->128	0.10264
125 ->127	0.29117
125 ->129	0.10664
126 ->128	0.16332
126 ->131	0.13422

Calculated triplet excited-states of *fac*-[Re(bqp-κ²*N*)(CO)₃(NC₅H₅)]⁺ in CH_3CN. The excited state number is followed by the spin multiplicity, symmetry, excitation energy, and oscillator strength *f*. The excitations from occupied to virtual orbitals are listed on the next line, followed by the wavefunction coefficients.

Excited State 1: Triplet-A 2.4883 eV 498.26 nm f=0.0000 <S**2>=2.000
127 ->137 -0.12089
129 ->142 0.10540
130 ->137 -0.11249
132 ->137 -0.23821
134 ->137 0.35680
135 ->137 -0.18350
136 ->137 0.44460
This state for optimization and/or second-order correction.
Total Energy, E(TD-HF/TD-KS) = -1717.04968353
Copying the excited state density for this state as the 1-particle RhoCI density.

Excited State 2: Triplet-A 2.7935 eV 443.83 nm f=0.0000 <S**2>=2.000
131 ->146 -0.14228
134 ->138 -0.28461
134 ->140 0.31433
136 ->138 0.34304
136 ->140 -0.33761

Excited State 3: Triplet-A 3.1911 eV 388.54 nm f=0.0000 <S**2>=2.000
132 ->137 0.19965
135 ->137 0.51732
136 ->137 0.33381

Excited State 4: Triplet-A 3.3577 eV 369.25 nm f=0.0000 <S**2>=2.000
129 ->137 -0.30457
132 ->137 0.36250
133 ->137 0.11245
134 ->137 -0.16879
135 ->137 -0.35964
136 ->137 0.24972

Excited State 5: Triplet-A 3.4272 eV 361.77 nm f=0.0000 <S**2>=2.000
129 ->137 -0.25076
133 ->137 0.52403
134 ->137 0.23661
136 ->137 -0.14601

Excited State 6: Triplet-A 3.5138 eV 352.85 nm f=0.0000 <S**2>=2.000
127 ->137 0.19200
132 ->141 -0.10151
133 ->137 0.30560
134 ->139 0.11185
135 ->137 0.11196
135 ->138 -0.18364
136 ->137 0.23290
136 ->138 0.19443
136 ->139 0.24698

Excited State 7: Triplet-A 3.5806 eV 346.27 nm f=0.0000 <S**2>=2.000
125 ->139 -0.10187
128 ->144 0.16040
129 ->137 0.17140
133 ->137 0.10455
134 ->137 -0.14195
134 ->138 0.11151
135 ->138 0.34863
135 ->139 -0.16465
135 ->140 0.22580
136 ->137 0.12848
136 ->138 0.20736
136 ->140 0.12352

Excited State 8: Triplet-A 3.6334 eV 341.23 nm f=0.0000 <S**2>=2.000
129 ->137 0.45009
133 ->137 0.22143
134 ->137 -0.13755
134 ->138 -0.12393
135 ->137 -0.17131
135 ->139 0.18992
136 ->138 -0.15899
136 ->140 -0.11165

Excited State 9: Triplet-A 3.6975 eV 335.32 nm f=0.0000 <S**2>=2.000

129 ->137	0.22972
132 ->137	0.33671
134 ->137	0.40339
135 ->139	-0.18965
136 ->138	-0.10812

Calculated triplet excited-states of *fac*-[Re(bqp-κ²*N*)(CO)₃(PPh₃)]⁺ in CH_3CN. The excited state number is followed by the spin multiplicity, symmetry, excitation energy, and oscillator strength *f*. The excitations from occupied to virtual orbitals are listed on the next line, followed by the wavefunction coefficients.

Excited State 1: Triplet-A 2.5473 eV 486.73 nm f=0.0000 <S**2>=2.000
170 ->185 0.13852
174 ->185 -0.12043
176 ->185 -0.10127
177 ->185 -0.13226
178 ->185 -0.10007
183 ->185 0.48567
184 ->185 0.35458
This state for optimization and/or second-order correction.
Total Energy, E(TD-HF/TD-KS) = -2505.03574436
Copying the excited state density for this state as the 1-particle RhoCI density.

Excited State 2: Triplet-A 2.7761 eV 446.61 nm f=0.0000 <S**2>=2.000
178 ->186 -0.10857
183 ->186 -0.28259
183 ->187 0.21320
184 ->186 0.44051
184 ->187 -0.30745

Excited State 3: Triplet-A 3.2999 eV 375.72 nm f=0.0000 <S**2>=2.000
170 ->185 0.10503
171 ->185 -0.13480
176 ->185 0.12628
178 ->185 0.18638
181 ->185 -0.15922
182 ->185 0.26091
183 ->185 -0.10547
183 ->186 -0.12408
183 ->187 -0.12397
183 ->190 -0.12576
184 ->185 0.36329

Excited State 4: Triplet-A 3.4042 eV 364.21 nm f=0.0000 <S**2>=2.000

171 ->185	0.10324
176 ->185	-0.10783
178 ->185	-0.13134
181 ->185	-0.11634
182 ->185	0.35195
182 ->186	0.16091
182 ->187	0.11192
183 ->185	0.20444
184 ->185	-0.33475
184 ->187	-0.12031

Excited State 5: Triplet-A 3.4795 eV 356.32 nm f=0.0000 <S**2>=2.000

171 ->185	0.40715
180 ->185	-0.28617
181 ->185	-0.38269
182 ->185	-0.12229
183 ->185	-0.12692

Excited State 6: Triplet-A 3.5981 eV 344.58 nm f=0.0000 <S**2>=2.000

170 ->185	-0.20040
171 ->185	0.10734
181 ->185	-0.10922
182 ->185	0.38575
182 ->186	-0.12012
183 ->186	0.21892
183 ->187	0.18055
183 ->190	0.10229
184 ->185	0.17417
184 ->186	0.15840
184 ->187	0.15251

Excited State 7: Triplet-A 3.6149 eV 342.98 nm f=0.0000 <S**2>=2.000

171 ->185	0.22706
172 ->194	-0.13645
176 ->185	-0.13121
176 ->197	-0.13214
180 ->194	-0.11077
181 ->185	0.26946
181 ->188	0.11616
181 ->189	0.14810
181 ->194	0.15670
183 ->185	-0.19384
184 ->185	0.16872

Calculated triplet excited-states of *fac*-[Re(bqp-κ^3*N*)(CO)$_3$]$^+$ in CH_3CN. The excited state number is followed by the spin multiplicity, symmetry, excitation energy, and oscillator strength *f*. The excitations from occupied to virtual orbitals are listed on the next line, followed by the wavefunction coefficients.

Excited State 1: Triplet-A 2.4093 eV 514.60 nm f=0.0000 <S**2>=2.000
111 ->117 0.23437
112 ->116 -0.16114
114 ->117 0.23929
115 ->116 0.56735
This state for optimization and/or second-order correction.
Total Energy, E(TD-HF/TD-KS) = -1468.76243265
Copying the excited state density for this state as the 1-particle RhoCI density.

Excited State 2: Triplet-A 2.4495 eV 506.16 nm f=0.0000 <S**2>=2.000
111 ->116 0.26296
112 ->117 -0.15856
114 ->116 0.34593
115 ->117 0.47606

Excited State 3: Triplet-A 3.1290 eV 396.25 nm f=0.0000 <S**2>=2.000
111 ->116 -0.10650
113 ->116 0.29310
114 ->116 0.53732
115 ->117 -0.23121
115 ->119 0.14836

Excited State 4: Triplet-A 3.1947 eV 388.09 nm f=0.0000 <S**2>=2.000
111 ->116 0.12253
113 ->116 0.52239
114 ->116 -0.26076
114 ->118 -0.16384
115 ->117 0.23328
115 ->119 0.11587

Excited State 5: Triplet-A 3.2294 eV 383.92 nm f=0.0000 <S**2>=2.000
108 ->116 0.14215
113 ->117 0.10875
114 ->117 0.52890
114 ->119 0.13180
115 ->116 -0.27599
115 ->118 -0.23875

Excited State 6: Triplet-A 3.2939 eV 376.41 nm f=0.0000 <S**2>=2.000
109 ->117 -0.17547
110 ->116 0.15932
112 ->116 0.58686
115 ->116 0.21857
115 ->118 -0.12115

Excited State 7: Triplet-A 3.3560 eV 369.44 nm f=0.0000 <S**2>=2.000
108 ->117 0.12485
109 ->116 -0.25856
110 ->117 0.20038
112 ->117 0.30690
113 ->116 -0.30613
114 ->118 -0.15374
115 ->119 0.30932

Excited State 8: Triplet-A 3.4824 eV 356.03 nm f=0.0000 <S**2>=2.000
109 ->117 0.19645
110 ->116 -0.27290
113 ->117 0.57910
115 ->116 0.11104
Excited State 9: Triplet-A 3.5213 eV 352.10 nm f=0.0000 <S**2>=2.000
108 ->117 0.14717
109 ->116 0.26425
110 ->117 -0.20602
111 ->116 0.31008
112 ->117 -0.19689
112 ->119 -0.13486
113 ->116 -0.15132
114 ->118 -0.20946
115 ->117 -0.23744
115 ->119 0.14217

Excited State 10: Triplet-A 3.6091 eV 343.53 nm f=0.0000 <S**2>=2.000

108 ->116	-0.14351
109 ->117	-0.13195
110 ->116	0.15851
111 ->117	-0.23378
114 ->117	0.31757
115 ->118	0.49181

Appendix C

Mulliken Population Analyses of Re(I) Complexes

The Fragment Analysis Based on Mulliken Populations for *fac*-Re(bqp-κ^2N)(CO)$_3$Cl (**1**) in the Singlet Ground State.[a]

Molecular Orbital	E, eV	Re									CO[b]	bqp-κ^2N[c]	Cl[d]
		s	p_x	p_y	p_z	d_{z^2}	d_{xz}	d_{yz}	$d_{x^2-y^2}$	d_{xy}	$\Sigma_{s,p,d}$	$\Sigma_{s,p,d}$	$\Sigma_{s,p,d}$
119 (O)	-6.89	0.02	0.03	0.00	0.11	0.09	-0.01	0.46	0.00	0.16	0.53	98.15	0.44
120 (O)	-6.77	0.02	0.01	0.05	0.03	1.37	0.00	3.15	0.02	0.24	2.13	83.70	9.29
121 (O)	-6.35	0.06	0.18	0.00	-0.01	0.06	0.02	0.52	0.35	1.40	2.57	94.50	0.33
122 (O)	-5.88	0.18	0.06	-0.01	0.03	4.19	0.12	15.29	4.83	37.78	26.12	11.24	0.16
123 (O)	-5.04	0.04	0.61	2.26	0.08	18.24	0.02	9.97	0.27	9.72	20.38	2.84	35.56
124 (O)	-4.90	0.00	1.23	0.51	0.02	6.54	13.20	11.04	11.05	0.00	20.96	3.82	31.62
125 (V)	-2.40	0.03	0.32	0.05	0.04	0.09	0.01	0.14	0.40	0.00	1.11	97.52	0.29
126 (V)	-1.78	0.03	0.05	0.13	0.07	0.00	0.16	0.00	0.00	0.06	1.09	98.40	-0.01
127 (V)	-1.42	0.03	0.40	0.05	0.01	0.03	0.56	0.01	0.00	0.25	1.72	96.94	0.01

[a]The orbital occupancy status is given in parenthesis (O = occupied, V = virtual). [b]Sum of the percent population for the three carbon and three oxygen atoms present in the three carbonyl (CO) ligands. [c]Sum of the percent populations for the twenty-three carbon, three nitrogen, and fifteen hydrogen atoms present in the 2,6-bis(quinoline)pyridine (bqp-κ^2N) ligand. [d]Sum of the percent populations for the one chlorine atom present in the chloride ligand

The Fragment Analysis Based on Mulliken Populations for *fac*-[Re(bqp-κ^2N)(CO)$_3$(NCCH$_3$)]$^+$ (**2**) in the Singlet Ground State.[a]

		Re									CO[b]	bqp-κ^2N[c]	CH_3CN[d]
Molecular Orbital	E, eV	s	p_x	p_y	p_z	d_{z^2}	d_{xz}	d_{yz}	$d_{x^2-y^2}$	d_{xy}	$\Sigma_{s,p,d}$	$\Sigma_{s,p,d}$	$\Sigma_{s,p,d}$
123 (O)	-9.01	0.04	0.08	0.18	0.03	15.05	7.17	4.88	11.10	3.34	13.94	38.36	5.83
124 (O)	-8.85	0.01	-0.10	0.04	-0.08	2.71	0.03	32.45	1.19	16.74	17.62	19.81	9.57
125 (O)	-8.75	0.02	0.05	0.80	0.00	5.60	0.24	0.61	0.09	17.59	13.39	59.54	2.07
126 (O)	-8.49	-0.01	0.03	0.14	0.19	7.74	0.19	2.82	0.09	9.77	6.64	71.33	1.08
127 (V)	-5.53	-0.05	0.87	0.80	0.02	0.14	0.12	0.11	0.08	0.09	9.22	88.42	0.17
128 (V)	-4.52	0.02	1.48	0.10	0.08	0.01	0.05	0.04	0.10	0.05	14.78	82.58	0.71

[a]The orbital occupancy status is given in parenthesis (O = occupied, V = virtual). [b]Sum of the percent population for the three carbon and three oxygen atoms present in the three carbonyl (CO) ligands. [c]Sum of the percent populations for the twenty-three carbon, three nitrogen, and fifteen hydrogen atoms present in the 2,6-bis(quinoline)pyridine (bqp-κ^2N) ligand. [d]Sum of the percent populations for the two carbon, three hydrogen, and one nitrogen atoms present in the acetonitrile ligand.

The Fragment Analysis Based on Mulliken Populations for *fac*-[Re(bqp-κ^2N)(CO)$_3$(NC$_5$H$_5$)]$^+$ (**3**) in the Singlet Ground State.[a]

Molecular Orbital	E, eV	Re									CO[b]	bqp-κ^2N[c]	NC$_5$H$_5$[d]
		s	p_x	p_y	p_z	d_{z^2}	d_{xz}	d_{yz}	$d_{x^2-y^2}$	d_{xy}	$\Sigma_{s,p,d}$	$\Sigma_{s,p,d}$	$\Sigma_{s,p,d}$
133 (O)	-9.11	0.08	0.84	0.19	0.06	17.51	6.44	17.69	1.04	20.90	26.04	8.74	0.47
134 (O)	-9.01	0.07	-0.03	0.65	-0.05	1.97	1.49	21.92	0.80	5.76	14.98	52.08	0.36
135 (O)	-8.92	-0.01	-0.04	0.24	0.07	16.90	2.94	2.01	18.76	20.01	24.83	9.10	5.17
136 (O)	-8.66	0.07	0.05	0.02	0.28	8.92	0.08	10.66	0.11	1.95	7.95	69.58	0.32
137 (V)	-5.18	-0.05	0.18	0.56	0.15	0.01	0.20	0.24	0.08	0.03	1.94	96.21	0.47
138 (V)	-4.46	0.00	0.94	0.56	0.95	0.28	0.15	0.01	0.09	0.14	4.39	8.99	83.50

[a]The orbital occupancy status is given in parenthesis (O = occupied, V = virtual). [b]Sum of the percent population for the three carbon and three oxygen atoms present in the three carbonyl (CO) ligands. [c]Sum of the percent populations for the twenty-three carbon, three nitrogen, and fifteen hydrogen atoms present in the 2,6-bis(quinoline)pyridine (bqp-κ^2N) ligand. [d]Sum of the percent populations for the five carbon, five hydrogen, and one nitrogen atoms present in the pyridine ligand.

The Fragment Analysis Based on Mulliken Populations for *fac*-[Re(bqp-κ^2N)(CO)$_3$(PPh$_3$)]$^+$ (**4**) in the Singlet Ground State.[a]

		Re									CO[b]	bqp-κ^2N[c]	PPh$_3$[d]
Molecular Orbital	E, eV	s	p_x	p_y	p_z	d_{z^2}	d_{xz}	d_{yz}	$d_{x^2-y^2}$	d_{xy}	$\Sigma_{s,p,d}$	$\Sigma_{s,p,d}$	$\Sigma_{s,p,d}$
181 (O)	-8.92	0.00	0.49	0.18	-0.01	2.97	0.20	2.95	0.01	2.06	2.60	86.80	1.77
182 (O)	-8.50	0.09	-0.08	0.56	0.14	0.02	0.05	0.80	4.53	10.90	9.37	69.46	4.17
183 (O)	-8.27	0.46	0.27	0.45	0.82	5.99	3.17	0.46	20.83	4.35	14.49	24.96	23.76
184 (O)	-8.19	0.09	0.03	0.01	0.16	6.44	3.49	9.14	0.11	12.50	10.98	48.32	8.73
185 (V)	-5.15	-0.01	0.45	0.80	0.16	0.07	0.44	0.06	0.43	0.07	10.19	82.46	4.88
186 (V)	-4.33	0.02	2.04	0.21	0.07	0.11	0.03	0.02	-0.01	0.03	19.47	46.91	30.00

[a]The orbital occupancy status is given in parenthesis (O = occupied, V = virtual). [b]Sum of the percent population for the three carbon and three oxygen atoms present in the three carbonyl (CO) ligands. [c]Sum of the percent populations for the twenty-three carbon, three nitrogen, and fifteen hydrogen atoms present in the 2,6-bis(quinoline)pyridine (bqp-κ^2N) ligand. [d]Sum of the percent populations for the eighteen carbon, fifteen hydrogen, and one phosphorous atoms present in the triphenyl phosphine ligand.

The Fragment Analysis Based on Mulliken Populations for *fac*-[Re(bqp-κ^3*N*)(CO)$_3$]$^+$ in the Singlet Ground State.[a]

		Re									CO[b]	bqp-κ^3*N*[c]
Molecular Orbital	E, eV	s	p_x	p_y	p_z	d_{z^2}	d_{xz}	d_{yz}	$d_{x^2-y^2}$	d_{xy}	$\Sigma_{s,p,d}$	$\Sigma_{s,p,d}$
112 (O)	-9.64	0.07	0.05	0.10	0.08	3.88	4.56	9.13	7.02	4.75	12.96	57.38
113 (O)	-9.43	0.16	0.78	1.02	0.21	0.08	0.40	7.59	5.44	37.54	24.09	22.69
114 (O)	-9.21	0.01	-0.06	-0.01	0.18	15.51	3.25	5.44	9.66	0.00	13.16	52.86
115 (O)	-9.10	0.03	-0.13	0.16	0.68	20.25	0.41	21.57	1.90	2.87	18.41	33.85
116 (V)	-5.34	0.01	0.59	0.46	0.14	0.00	0.39	0.27	0.01	0.00	2.35	95.77
117 (V)	-4.94	0.02	0.02	0.17	0.30	0.08	0.70	0.00	0.12	0.09	1.49	97.01

[a]The orbital occupancy status is given in parenthesis (O = occupied, V = virtual). [b]Sum of the percent population for the three carbon and three oxygen atoms present in the three carbonyl (CO) ligands. [c]Sum of the percent populations for the twenty-three carbon, three nitrogen, and fifteen hydrogen atoms present in the 2,6-bis(quinoline)pyridine (bqp-κ^3*N*) ligand.

Appendix D

Optimized Geometry of Re(I) Complexes

fac-Re(bqp-κ²*N*)(CO)₃Cl

Atom	Coordinates		
	X	Y	Z
Re	1.89041	0.44687	-2.7169
C	3.48216	0.23626	-1.6933
C	1.53166	-1.3623	-2.196
C	2.82941	-0.1582	-4.3121
O	1.43932	-2.4559	-1.8062
O	3.43752	-0.5082	-5.2371
O	4.46137	0.07462	-1.0793
N	2.5104	2.59207	-3.2632
C	2.15973	3.16743	-4.4631
C	3.55065	3.10321	-2.6032
C	0.94607	2.80886	-5.1232
C	3.00642	4.15818	-5.0665
C	4.36349	4.14493	-3.0803
H	3.78371	2.65353	-1.6497
C	0.72623	3.31331	-6.4042
C	-0.1926	2.0226	-4.5593
C	2.72178	4.65133	-6.3644
C	4.12024	4.63898	-4.3375
H	5.18678	4.49711	-2.4695
C	1.61369	4.2033	-7.0404
H	-0.1702	3.01358	-6.9357
C	-1.4705	2.56064	-4.7838
N	-0.0298	0.79403	-3.9961
H	3.39404	5.38184	-6.8045
H	4.75865	5.39708	-4.7816
H	1.39381	4.55102	-8.0444
C	-2.5994	1.78407	-4.5686
H	-1.5604	3.57988	-5.1379
C	-1.1244	-0.0199	-3.9392
C	-2.4122	0.45619	-4.2111
H	-3.5937	2.18821	-4.7292
C	-1.012	-1.4847	-3.6857
H	-3.2487	-0.2292	-4.1457
C	-0.3096	-2.3255	-4.6148
C	-1.7557	-2.0736	-2.6762

C	-0.3369	-3.7447	-4.4184
N	0.32909	-1.7572	-5.6781
C	-1.7767	-3.4742	-2.4886
H	-2.3272	-1.4437	-2.0024
C	-1.0712	-4.2965	-3.3366
C	0.36493	-4.5527	-5.3504
C	0.95908	-2.5498	-6.5254
H	-2.3554	-3.8929	-1.6709
H	-1.0793	-5.375	-3.2021
C	1.01912	-3.9594	-6.4039
H	0.36755	-5.6319	-5.2211
H	1.45455	-2.0627	-7.364
H	1.56291	-4.5445	-7.1384
Cl	0.80883	1.28655	-0.9063

fac-[Re(bqp-κ^2*N*)(CO)$_3$(NCCH$_3$)]$^+$

Atom	Coordinates		
	X	Y	Z
Re	1.19827	-0.1381	0.07812
N	1.43959	1.88861	-0.0307
C	1.38495	2.6051	1.11009
C	1.6208	2.60897	-1.2131
C	1.2731	1.99715	2.50631
C	1.38215	4.00989	1.11783
C	2.03737	2.06718	-2.5828
C	1.46004	4.00861	-1.2436
C	0.52341	0.86338	2.74587
C	1.91381	2.65282	3.54818
C	1.36813	4.7174	-0.066
H	1.36731	4.53602	2.0496
C	3.38023	1.72853	-2.8298
C	1.08856	1.97791	-3.6014
H	1.45421	4.53216	-2.1786
C	0.11885	0.60669	4.06638
N	0.14584	0.05404	1.76707
C	1.69971	2.24853	4.86229
H	2.57529	3.46502	3.33441

H	1.29248	5.7879	-0.0645
C	3.76221	1.34419	-4.1229
N	4.30438	1.85381	-1.8568
C	1.45423	1.48422	-4.8556
H	0.07714	2.27175	-3.4122
C	0.75077	1.25989	5.12814
C	-0.9202	-0.2864	4.30573
C	-0.9578	-0.7254	1.93313
H	2.25082	2.70099	5.65808
C	2.79486	1.17788	-5.1232
C	5.11795	1.16167	-4.4154
C	5.62389	1.77823	-2.1358
H	0.70952	1.34242	-5.6097
H	0.50968	1.00436	6.1361
C	-1.5235	-0.901	3.21477
H	-1.2502	-0.4861	5.30474
H	-1.4058	-1.2197	1.0946
H	3.07974	0.82622	-6.0925
C	6.06116	1.41187	-3.4171
H	5.42916	0.84878	-5.3905
H	6.34464	2.00215	-1.3752
H	-2.3446	-1.5079	3.35126
H	7.10862	1.32701	-3.6282
C	2.9402	-0.3076	1.14291
O	3.99997	-0.4643	1.80588
C	2.29303	-0.5403	-1.6076
O	3.0014	-0.8427	-2.6013
C	0.8464	-2.1469	0.24789
O	0.62969	-3.384	0.35243
N	-0.3395	-0.4212	-1.0437
C	-1.1646	-0.9897	-1.5052
C	-2.218	-1.9403	-2.0177
H	-2.8599	-1.4625	-2.7189
H	-1.7184	-2.762	-2.4922
H	-2.7877	-2.2928	-1.1876

fac-[Re(bqp-κ²*N*)(CO)₃(NC₅H₅)]⁺

Atom	Coordinates		
	X	Y	Z
Re	1.19716	-0.29472	-0.05859
N	1.5154	1.96554	-0.07779
C	1.38063	2.64355	1.10129
C	1.68951	2.69408	-1.21768
C	1.30808	1.97258	2.43392
C	1.28993	4.04326	1.13067
C	2.02811	2.06425	-2.53219
C	1.61701	4.08984	-1.22426
C	0.4063	0.90856	2.73864
C	1.99368	2.56275	3.49007
C	1.39029	4.77809	-0.04176
H	1.1149	4.54193	2.07503
C	3.4099	1.85393	-2.84846
C	1.07134	1.88349	-3.514
H	1.74593	4.6142	-2.16371
C	0.07332	0.63675	4.10234
N	-0.14068	0.15957	1.72551
C	1.77074	2.19632	4.83482
H	2.70776	3.35186	3.27874
H	1.3043	5.85963	-0.02935
C	3.76226	1.42568	-4.16748
N	4.34566	2.07562	-1.87926
C	1.4251	1.44288	-4.81175
H	0.02974	2.09447	-3.29455
C	0.7869	1.28439	5.14275
C	-0.97428	-0.27999	4.36424
C	-1.1453	-0.66984	2.01234
H	2.34474	2.67864	5.61909
C	2.74399	1.21877	-5.13463
C	5.1394	1.23112	-4.44799
C	5.61538	1.88146	-2.18776
H	0.64566	1.29695	-5.55319
H	0.54704	1.04541	6.17411
C	-1.62559	-0.88793	3.31502
H	-1.25614	-0.48515	5.39291

H	-1.56724	-1.22185	1.17974
H	3.02396	0.89063	-6.13215
C	6.06949	1.45783	-3.4609
H	5.44051	0.90602	-6.13215
H	6.33887	2.06712	-1.39517
H	-2.45136	-1.57194	3.47258
H	7.13115	1.32089	-3.63831
C	2.7567	-0.54477	1.04949
O	3.70495	-0.71633	-1.69687
C	2.25974	-0.79507	-1.57838
O	2.87225	-1.20606	-2.47669
C	0.77786	-2.16058	0.11985
O	0.53069	-3.2894	0.24242
N	-0.6627	0.07389	-1.28501
C	-1.50715	1.08755	-0.99556
C	-0.9661	-0.71806	-2.33915
C	-2.65715	1.34484	-1.73501
H	-1.24613	1.70409	-0.14509
C	-2.09707	-0.52704	-3.12302
H	-0.27339	-1.52255	-2.55353
C	-2.96275	0.52431	-2.81975
H	-3.29488	2.17591	-1.45527
H	-2.28664	-1.19574	-3.95529
H	-3.85288	0.69922	-3.41553

fac-[Re(bqp-κ^2*N*)(CO)$_3$(PPh$_3$)]$^+$

Atom	Coordinates		
	X	Y	Z
Re	0.66746	-0.62419	0.27804
N	1.28265	1.28434	0.56862
C	1.0816	1.87848	1.76601
C	1.8675	2.06244	-0.42336
C	0.5407	1.18	2.9837
C	1.3245	3.24865	1.96405
C	2.5108	1.60141	-1.73604
C	1.9515	3.4674	-0.29885
C	-0.4315	0.17767	2.89163

C	1.0125	1.62537	4.22513
C	1.7017	4.06124	0.91214
H	1.1788	3.68752	2.93596
C	3.7873	1.0374	-1.7285
C	1.8180	1.81296	-2.93661
H	2.2388	4.07765	-1.12765
C	-1.1561	-0.07995	4.05789
N	-0.7052	-0.46532	1.73181
C	0.4410	1.16139	5.40181
H	1.8132	2.31832	4.26161
H	1.7976	5.12546	1.04386
C	4.3851	0.71975	-2.94553
N	4.4474	0.88513	-0.57265
C	2.3702	1.37212	-4.13626
H	0.8463	2.29217	-2.92911
C	-0.6874	0.34941	5.31719
C	-2.3437	-0.7611	3.96911
C	-1.9518	-1.02001	1.58534
H	0.8600	1.42661	6.34858
C	3.6653	0.84094	-4.14543
C	5.7198	0.3192	-2.96628
C	5.7750	0.61659	-0.57041
H	1.8080	1.44023	-5.04046
H	-1.19746	0.05848	6.21591
C	-2.79828	-1.15979	2.70116
H	-2.91557	-0.97661	4.85128
H	-2.28938	-1.34282	0.62571
H	4.11468	0.53885	-5.07014
C	6.43361	0.29714	-1.76634
H	6.19662	0.05287	-3.88785
H	6.33962	0.649	0.33838
H	-3.77078	-1.57226	2.60317
H	7.47892	0.04149	-1.76583
C	1.99492	-1.15115	1.76455
O	2.80183	-1.47147	2.66816
C	1.98462	-1.17043	-1.18175
O	2.82518	-1.56311	-2.0193
C	0.00584	-2.60469	0.16944
O	-0.47042	-3.78008	0.0593
P	-0.56205	0.10076	-1.57208

C	-1.96832	-0.95954	-1.1492
C	-3.07243	-0.44027	-0.46169
C	-1.94453	-2.30427	-1.52901
C	-4.15512	-1.27972	-0.16919
H	-3.09813	0.59096	-0.16658
C	-3.01849	-3.14491	-1.20944
H	-1.10086	-2.6941	-2.06192
C	-4.12699	-2.63183	-0.53708
H	-5.00783	-0.8904	0.33591
H	-2.99144	-4.18142	-1.47876
H	-4.95716	-3.27093	-0.30135
C	0.01404	-0.33252	-3.25461
C	0.8728	-1.41697	-3.45924
C	-0.40406	0.43815	-4.35772
C	1.30424	-1.74431	-4.7548
H	1.19358	-2.00168	-2.62499
C	0.0509	0.12392	-5.64549
H	-1.06695	1.26991	-4.21771
C	0.90004	-0.96973	-5.84525
H	1.93935	-2.591	-4.91222
H	-0.25402	0.71819	-6.47806
H	1.2356	-1.21191	-6.83201
C	-1.09391	1.83543	-1.54837
C	-0.96363	2.6439	-2.68124
C	-1.61458	2.36308	-0.36817
C	-1.37737	3.97705	-2.63488
H	-0.55522	2.23985	-3.57703
C	-1.998	3.70086	-0.30222
H	-1.69802	1.74015	0.49452
C	-1.89088	4.50712	-1.44087
H	-1.30341	4.58659	-3.50955
H	-2.37539	4.10178	0.61596
H	-2.19523	5.52662	-1.39972

fac-[Re(bqp-κ^3*N*)(CO)$_3$]$^+$

Atom	Coordinates		
	X	Y	Z
Re	1.20281	-0.2903	-0.0737
N	1.51683	1.97056	-0.0869
C	1.37556	2.64794	1.09168
C	1.6941	2.69893	-1.2261
C	1.30139	1.97592	2.42394
C	1.28196	4.04743	1.12015
C	2.03856	2.06729	-2.5378
C	1.61977	4.09461	-1.2331
C	0.4066	0.90485	2.72489
C	1.97917	2.56979	3.48314
C	1.3861	4.78226	-0.0518
H	1.10272	4.5462	2.06367
C	1.26891	0.93881	-2.9708
C	3.18858	2.40967	-3.2251
H	1.75357	4.61926	-2.1716
C	0.07368	0.62544	4.08699
N	-0.134	0.15529	1.70894
C	1.75647	2.19733	4.82644
H	2.68816	3.36443	3.27546
H	1.30021	5.86393	-0.039
C	1.69286	0.21315	-4.1287
N	0.15757	0.5911	-2.2579
C	3.59264	1.69848	-4.3805
H	3.80234	3.23115	-2.8696
C	0.78192	1.27606	5.13035
C	-0.9672	-0.3003	4.34393
C	-1.1341	-0.6811	1.99049
H	2.32488	2.68157	5.61354
C	2.86117	0.62045	-4.8246
C	0.90975	-0.9008	-4.5277
C	-0.5395	-0.4534	-2.6677
H	4.49329	2.0044	-4.9038
H	0.5417	1.03065	6.16048
C	-1.6134	-0.9083	3.2916
H	-1.2472	-0.5121	5.37168

H	-1.5513	-1.2313	1.15457
H	3.17114	0.06325	-5.7048
C	-0.2077	-1.237	-3.8001
H	1.2045	-1.4728	-5.4035
H	-1.4197	-0.7079	-2.079
H	-2.4341	-1.5993	3.44445
H	-0.8309	-2.0819	-4.0743
C	2.75999	-0.532	1.03865
O	3.69928	-0.6857	1.7031
C	2.26361	-0.7905	-1.5957
O	2.87521	-1.2036	-2.4935
C	0.78701	0.10417	-2.1564
O	0.53671	-3.284	0.2309

REFERENCES

1. Rohatgi-Mukherjee, K. K. *Fundamentals of Photochemistry*; John Wiley & Sons: New York, 1978; pgs 211–212, 268–270. (b) Calvert, J. G.; Pitts Jr., J. N. *Photochemistry*; John Wiley & Sons: New York, 1966; pgs 19–21.
2. Ferraudi, G. J. *Elements of Inorganic Photochemistry*; John Wiley & Sons: New York, 1988; pgs 7–8.
3. Davidson, J. L.; Sharp, D. W. A. *J. Chem. Soc. Dalton* **1973**, 1957–1960. (b) Davidson, J. L.; Sharp, D. W. A. *J. Chem. Soc. Dalton* **1972**, 107–109.
4. Wrighton, M. S.; Ginley, D. S. *J. Am. Chem. Soc.* **1975**, *97*, 4246–4251. (b) Wrighton, M. S.; Ginley, D. S. *J. Am. Chem. Soc.* **1975**, *97*, 2065–2072.
5. Endicott, J. F. *J. Chem. Edu.***1983**, *60*, 824–829.
6. Abrahamsson, M.; Jäger, M.; Österman, T.; Eriksson, L.; Persson, P.; Becker, H.-C.; Johannsson, O.; Hammarström, L. *J. Am. Chem. Soc*. **2006**, *128*, 12616–12617.
7. Abrahamsson, M.; Jäger, M.; Kumar, R. J.; Österman, T.; Persson, P.; Becker, H.-C.; Johannsson, O.; Hammarström, L. *J. Am. Chem. Soc*. **2008**, *130*, 15533–15542.
8. Demas, J. N.; Harris, E. W.; Flynn Jr., C. M.; Diemente, D. *J. Am. Chem. Soc.* **1975**, *97*, 3838–3839.
9. Nallas, G. N. A.; Jones, S. W.; Brewer, K. J. *Inorg. Chem.* **1996**, *35*, 6974–6980.
10. Black, D. R.; Hightower, S. E., *Inorg. Chem.* **2011**, *submitted and under review*.
11. Amoroso, A. J.; Banu, A.; Coogan, M. P.; Edwards, P. G.; Hossain, G.; Abdul Malik, K. M. *Dalton Trans.* **2010**, *39*, 6993–7003.
12. Kirgan, R.; Simpson, M.; Moore, C.; Day, J.; Bui, L.; Tanner, C.; Rillema, D. P. *Inorg. Chem.* **2007**, *46*, 6464–6472.
13. Hightower, S. E.; Black, D. R. *Inorg. Chem.* **2011**, *submitted and under review*.
14. Sauvage, J.-P.; Collin, J.-P.; Chambron, J.-C.; Guillerez, S.; Courdet, C.; Balzani, V.; Barigelletti, F.; Decola, L.; Flamigni, L. *Chem. Rev.* **1994**, *94*, 993–1019.
15. Caspar, J. V.; Meyer, T. J. *J. Phys. Chem.* **1983**, *87*, 952–959.
16. Maestri, M.; Armaroli, N.; Balzani, V.; Constable, E. C.; Thompson, A. *Inorg. Chem.* **1995**, *34*, 2759–2767.

17. Wang, J. H.; Fang, Y. Q.; Hanan, G. S.; Loiseau, F.; Campagna, S. *Inorg. Chem.* **2005**, *44*, 5–7.
18. Medlycott, E. A.; Hanan, G. S. *Chem. Soc. Rev.* **2005**, *34*, 133–142.
19. Polson, M. I. J.; Loiseau, F.; Campagna, S.; Hana, G. S. *Chem. Comm.* **2006**, 1301–1303.
20. Hammarström, L.; Barigelletti, F.; Flamingni, L.; Indelli, M. T.; Armaroli, N.; Calogero, G.; Guardigli, M.; Sour, A.; Collin, J.-P.; Sauvage, J.-P. *J. Phys. Chem. A.* **1997**, *101*, 9061–9069. (b) Caspar, J. V.; Meyer, T. J. *J. Phys. Chem.* **1983**, *87*, 952–957.
21. Vogler, L. M.; Brewer, K. J. *Inorg. Chem.* **1996**, *35*, 818–824.
22. Son, S. U.; Park, K. H.; Lee, Y. S.; Kim, B. Y.; Choi, C. H.; Lah, M. S.; Jang, Y. H.; Jang, D. J.; Chung, Y. K. *Inorg. Chem.* **2004**, *43*, 6896–6898.
23. Duati, M.; Tasca, S.; Lynch, F. C.; Bohlen, H.; Vos, J. G.; Stagni, S.; Ward, M. D. *Inorg. Chem.* **2003**, *42*, 8377–8384.
24. Indelli, M. T.; Bignozzi, C. A.; Scandola, J. P.; Collin, J.-P. *Inorg. Chem.* **1998**, *37*, 6084–6089.
25. Wang, J. H.; Hanan, G. S.; Loiseau, F.; Campagna, S. *Chem. Comm.* **2004**, 2068–2069.
26. Baranoff, E.; Collin, J.-P.; Flamigni, L.; Sauvage, J.-P. *Chem. Soc. Rev.* **2004**, *33*, 147–155.
27. Stoyanov, S. R.; Villegas, J. M.; Cruz, A. J.; Lockyear, L. L.; Reibenspies, J. H.; Rillema, D. P. *J. Chem. Theory Comput.* **2005**, *1*, 95–105.
28. Sacsteder, L.; Zipp, A. P.; Brown, E. A.; Striech, J.; Demas, J. N.; DeGraff, B. A. *Inorg. Chem.* **1990**, *29*, 4335–4340. (b) Fredericks, S. M.; Luong, J. C.; Wrighton, M. S. *J. Am. Chem. Soc.* **1979**, *101*, 7415–7417.
29. ChemDoodleTM, version 4.1.1, http://www.chemdoodle.com/.
30. Klamt, A.; Schüürman, G. J. *J. Chem. Soc., Perkin Trans.* **1993**, *2*, 799. (b) Andzelm, J.; Kölmel, C.; Klamt, A. *J. Chem. Phys.* **1995**, *103*, 9312–9320. (c) Barone, V.;Cossi, M. *J. Chem. Phys. A* **1998**, *102*, 1995–2001. (d) Cossi, M.; Rega, N.; Scalmani, G.; Barone, V. *J. Comput. Chem.* **2003**, *24*, 669–681.
31. Becke, A. D. *Phys. Rev. A* **1988**, *38*, 3098–3100. (b) Becke, A. D. *J. Chem. Phys.* **1993**, *98*, 5648–5652. (c) Lee, C.; Yang, W.; Parr, R. G. *Phys. Rev. B* **1988**, *37*, 785–789. (d) Vosko, S. H.; Wilk, L.; Nusair, M. *Can. J. Phys.* **1980**, *58*, 1200–1211.

32. Gaussian 09, Revision A.1, Frisch, M. J.; Trucks, G. W.; Schlegel, H. B.; Scuseria, G. E.; Robb, M. A.; Cheeseman, J. R.; Scalmani, G.; Barone, V.; Mennucci, B.; Petersson, G. A.; Nakatsuji, H.; Caricato, M.; Li, X.; Hratchian, H. P.; Izmaylov, A. F.; Bloino, J.; Zheng, G.; Sonnenberg, J. L.; Hada, M.; Ehara, M.; Toyota, K.; Fukuda, R.; Hasegawa, J.; Ishida, M.; Nakajima, T.; Honda, Y.; Kitao, O.; Nakai, H.; Vreven, T.; Montgomery Jr., J. A.; Peralta, J. E.; Ogliaro, F.; Bearpark, M.; Heyd, J. J.; Brothers, E.; Kudin, K. N.; Staroverov, V. N.; Kobayashi, R.; Normand, J.; Raghavachari, K.; Rendell, A.; Burant, J. C.; Iyengar, S. S.; Tomasi, J.; Cossi, M.; Rega, N.; Millam, N. J.; Klene, M.; Knox, J. E.; Cross, J. B.; Bakken, V.; Adamo, C.; Jaramillo, J.; Gomperts, R.; Stratmann, R. E.; Yazyev, O.; Austin, A. J.; Cammi, R.; Pomelli, C.; Ochterski, J. W.; Martin, R. L.; Morokuma, K.; Zakrzewski, V. G.; Voth, G. A.; Salvador, P.; Dannenberg, J. J.; Dapprich, S.; Daniels, A. D.; Farkas, Ö.; Foresman, J. B.; Ortiz, J. V.; Cioslowski, J.; Fox, D. J. Gaussian, Inc., Wallingford CT, **2009**.
33. Dunning Jr., T. H.; Hay, P. J. In Modern Theoretical Chemistry; H. F. Schaefer, I., Ed.; Plenium: New York, **1976**, Vol. 3, 1.
34. Hay, P. J., Wadt, W. R. *J. Chem. Phys.* **1985**, *82*, 270–283.
35. Hay, P. J., Wadt, W. R. *J. Chem. Phys.* **1985**, *82*, 284–298.
36. Hay, P. J., Wadt, W. R. *J. Chem. Phys.* **1985**, *82*, 299–310.
37. McLean, A. D., Chandler, G. S. *J. Chem. Phys.* **1980**, *72*, 5639–5648. (b) Krishnan, R.; Binkley, J. S.; Seeger, R.; Pople, J. A. *J. Chem. Phys.* **1980**, *72*, 650–654.
38. Gorelsky, S. I.; Lever, A. B. P. *J. Organomet. Chem.* **2001**, *635*, 187–196.
39. Gorelsky, S. I. AOMix: Program for Molecular Orbital Analysis; York University: Toronto, Canada, **1997**; http://www.sg-chem.net/.
40. Mulliken, R. S. *J. Chem. Phys.* **1955**, *23*, 1833–1840.
41. Mulliken, R. S. *J. Chem. Phys.* **1955**, *23*, 1841–1845.
42. Mulliken, R. S. *J. Chem. Phys.* **1955**, *23*, 2338–2342.
43. Mulliken, R. S. *J. Chem. Phys.* **1955**, *23*, 2343–2346.
44. Reed, A. E.; Curtiss, L. A.; Weinhold, F. *Chem. Rev.* **1988**, *88*, 899–926.
45. Gorelsky, S. I.; Ghosh, S.; Solomon, E. I. *J. Am. Chem. Soc.* **2006**, *128*, 278–290.
46. Stratmann, R. E.; Scuseria, G. E.; Frisch, M. J. *J. Chem. Phys.* **1998**, *109*, 8218–8224. (b) Bauernschmitt, R.; Ahlrichs, R. *Chem. Phys. Lett.* **1996**, *256*, 454–464. (c) Casida, M. E.; Jamorski, C.; Casida, K. C.; Salahub, D. R. *J. Chem. Phys.* **1998**, *108*, 4439–4449.
47. Hatchard, C. G.; Parker, C. A. *Proc. Roy. Soc.* **1956**, *235*, 518–536.

48. Baxendale, J. H.; Bridge, N. K. *J. Phys. Chem. C* **1955**, *59*, 783–788.
49. Houk, L. W.; Dobson, G. R. *Inorg. Chem.* **1966**, *5*, 2119–2123.
50. Edwards, D. A.; Marshalsea, J. *J. Organomet. Chem.* **1977**, *131*, 73–91.
51. Giordano, P. J.; Wrighton, M. S. *J. Am. Chem. Soc.* **1979**, *101*, 2888–2897.
52. Gamelin, D. R.; George, M. W.; Glyn, P.; Grevels, F. W.; Johnson, F. P. A.; Klotzbücher, W.; Morrison, S. L.; Russell, G.; Schaffer, K.; Turner, J. J. *Inorg. Chem.* **1994**, *33*, 3246–3250.
53. Gabrielsson, A.; Blanco-Rodriguez, A. M.; Matousek, P.; Towrie, M.; Vlček Jr, A. *Organometallics* **2006**, *25*, 2148–2156.
54. Armarego, W. L. F.; Chai, L. L. Christina *Purification of the Laboratory Chemicals*; Elsevier: Oxford, 2009.
55. Morse, D. L.; Wrighton, M. S. *J. Am. Chem. Soc.* **1976**, *98*, 3931–3924.
56. Hepp, A. F.; Wrighton, M. S. *J. Am. Chem. Soc.* **1981**, *103*, 1258–1261.
57. Hughey, J. L. IV; Anderson, C. P.; Meyer, T. J. *J. Am. Chem. Soc.* **1975**, *97*, 4440–4441.
58. Waltz, W. L.; Hackelberg, O.; Dorfman, L. M.; Wojcicki, A. J. *J. Am. Chem. Soc.* **1978**, *100*, 7259–7264.
59. Hoffman, N. W.; Brown, T. L. *Inorg. Chem.* **1978**, *17*, 613–617. (b) Kidd, D. R.; Brown, T. L. *J. Am. Chem. Soc.* **1978**, *100*, 4095–4103. (c) Byers, B. H.; Brown, T. L. *J. Am. Chem. Soc.* **1977**, *99*, 2527–2532. (d) Absi-Halabi, M.; Brown T. L. *J. Am. Chem. Soc.*, **1977**, *99*, 2982–2988.
60. Watkins Jr, D. D.; George, T. A. *J. Organomet. Chem.* **1975**, *102*, 71–77.
61. Weinmann, D. J.; Abrahamson, H. B. *Inorg. Chem.* **1987**, *26*, 3034–3040.
62. Meyer, T. J.; Caspar, J. V. *Chem. Rev.* **1985**, *85*, 187–218.
63. Brandenburg, K. L.; Heeg, M. J.; Abrahamson, H. B. *Inorg. Chem.* **1987**, *26*, 246–259.
64. Weinmann, D. J. Doctoral Dissertation, University of North Dakota, **1988**.
65. Abrahamson, H. B.; Marxen, H. *Organometallics* **1993**, *12*, 2835–2840.
66. Weinmann, D. J.; Abrahamson, H. B. *Inorg. Chem.* **1987**, *26*, 2133–2137.
67. Hatchard, C. G.; Parker, C. A. *Proc. Roy. Soc.* **1956**, *235*, 518–536.